A Nonisolated Multiinput Multioutput DC–DC Boost Converter for Electric Vehicle Applications

Ali Nahavandi, Mehrdad Tarafdar Hagh, Mohammad Bagher Bannae Sharifian, and Saeed Danyali

***Abstract*—A new nonisolated multiinput multioutput dc–dc boost converter is proposed in this paper. This converter is applicable in hybridizing alternative energy sources in electric vehicles. In fact, by hybridization of energy sources, advantages of different sources are achievable. In this converter, the loads power can be flexibly distributed between input sources. Also, charging or discharging of energy storages by other input sources can be controlled properly. The proposed converter has several outputs with different voltage levels which makes it suitable for interfacing to multilevel inverters. Using of a multilevel inverter leads to reduction of voltage harmonics which, consequently, reduces torque ripple of electric motor in electric vehicles. Also, electric vehicles which using dc motor have at least two different dc voltage levels, one for ventilation system and cabin lightening and other for supplying electric motor. The proposed converter has just one inductor. Depending on charging and discharging states of the energy storage system (ESS), two different power operation modes are defined for the converter. In order to design the converter control system, small-signal model for each operation mode is extracted. The validity of the proposed converter and its control performance are verified by simulation and experimental results for different operation conditions.**

***Index Terms*—DC–DC converters, electric vehicle, hybrid power system, multiple-input–multiple-output (MIMO), small-signal modeling, state-space averaging.**

I. Introduction

INCREASING rapidly population and energy consumption in the world, increasing oil and natural gas prices, and the depletion of fossil fuels are justifiable reasons for using electrical vehicles (EVs) instead of fossil-fuel vehicles. The interest in developing the EVs with clean and renewable energy sources as a replacement for fossil-fuel vehicles has therefore steadily increased. The EVs are proposed as a potential and attractive solution for transportation applications to provide environmentally friendly operation with the usage of clean and renewable energy sources [1], [2]. In the EVs, the fuel cell (FC) stack usually used as clean energy source. The FCs are energy sources that directly convert the chemical energy reaction into the electrical energy. Currently, FCs are acknowledged as one of the promising technologies to meet the future energy generation requirements. FCs generate electric energy, rather than storing it, and continue to deliver the energy, as long as the fuel supply is maintained. However, there are some well-known technical limitations to FCs: they have slow power transfer rate in transitory situations, and a high cost per watt. This case is the reason for which FCs are not used alone in the EVs to satisfy the load demands, particularly during startup and transient events. So, in order to solve these problems, usually FC is used with energy storage systems (ESSs) such as batteries or supercapacitor (SC). Furthermore, the association of FC and ESSs leads to a reduction of the hydrogen consumption of the FC [3]–[7]. FC and ESSs such as battery and SC have different voltage levels. So, to provide a specific voltage level for load and control power flow between input sources, using of a dc–dc converter for each of the input sources is need. Usage of a dc–dc converter for each of the input sources leads to increase of price, mass, and losses. Consequently, in hybrid power systems, multiinput dc–dc converters have been used. Multiinput converters have two main types, isolated multiinput dc–dc converters and nonisolated multiinput dc–dc converters. In the following sections, two main types of multiinput converters are investigated.

In isolated multiinput dc–dc converters, high-frequency transformer is used in order to make electric isolation. High-frequency transformer provides electric isolation and impedance matching between two sides of converter. In general, isolated dc–dc converters use leakage inductance as energy storage for transferring power between two sides of converter. Usually isolated dc–dc converters, in addition to high-frequency transformer, have high-frequency inverter and rectifier. The power flow between input and output sides is controlled by adjusting the phase shift angle between primary and secondary voltages of transformer [8]–[10]. Isolated dc–dc converters have several types such as half-bridge isolated converters, full-bridge isolated converters, boost half-bridge isolated converters, and combinational multiport isolated converters [11]–[13]. Due to using of transformer, isolated dc–dc converters are heavy and massive. These converters require inverters in input sides of transformer for conversion of input dc voltage to ac and also need rectifiers in outputs of transformer for conversion of ac voltage to dc. Therefore, in all input and output terminals of these converters, several switches are applied which leads to increase of cost and losses. Furthermore, transformer has losses in its core and windings. Because of the aforementioned drawbacks of isolated multiinput dc–dc converters, usage of nonisolated multiinput dc–dc converters in electric vehicle applications seems more useful.

In [14], a nonisolated multiinput dc–dc converter which is derived from H-bridge structure has been proposed. In fact, by cascading two H-bridge with different dc-link voltages, different voltages due to addition or subtraction of H-bridges outputs

Manuscript received December 28, 2013; revised March 18, 2014; accepted May 6, 2014. Date of publication May 29, 2014; date of current version November 3, 2014. Recommended for publication by Associate Editor M. Ferdowsi.

A. Nahavandi, M. T. Hagh, and M. B. B. Sharifian are with the Faculty of Electrical and Computer Engineering, University of Tabriz, Tabriz, Iran (e-mail: ali_nahavandi@tabrizu.ac.ir; tarafdar@tabrizu.ac.ir; sharifian@tabrizu.ac.ir).

S. Danyali is with the Faculty of Engineering, University of Ilam, Ilam, Iran (e-mail: s.danyali90@gmail.com).

Color versions of one or more of the figures in this paper are available online at http://ieeexplore.ieee.org.

Digital Object Identifier 10.1109/TPEL.2014.2325830

are accessible. Modes in which either output voltage of the H-bridges is negative are not considered here because they are related to bidirectional double-input converters, which were beyond the scope of paper. By eliminating the aforementioned nonuseful modes, a simplified double input dc–dc converter is obtained. The advantage of this converter is its less number of passive elements, and its drawback is unsuitable control on the power which is drawn from input sources. In [15]–[17], a multiinput dc–dc buck converter is introduced. In fact, this converter consists of paralleling two buck converter in their inputs. One switch is series to each input source to prevent short circuit of sources. The advantage of this converter is reducing the number of inductors and capacitors which lead to reduction in cost, volume, and weight of converter. Lack of proper power flow control between input sources with each other is a shortcoming of the proposed converter. In [18], multiinput z-source dc–dc converter is presented. The structure of proposed converter is changed such that the number of inductors and capacitors is equal to a single input z-source converter. Nevertheless, two inductor and capacitor is applied in the proposed converter.

In [19], multiphase converter is introduced. The proposed converter has four input by different voltages. In this converter, each of the energy sources can deliver or absorb energy from load and other sources. Employment of a separate inductor for each input source is the drawback of this converter. In [20], a triple input converter for hybridization of battery, photovoltaic cells, and fuel cell is introduced by the author. By proper switching of converter, charge and discharge of battery by means of other sources and load is possible, respectively. In [21], a systematic approach for derivation of nonisolated multiinput converter topologies by combination of buck, boost, cuk, and sepic is presented. According to this paper, mentioned converters are divided to two types, pulsating voltage source converters (PVSC) and pulsating current source converters (PCSC). Because PVSC is considered as a voltage source, it can put series with current buffer (inductor) branch or output of other converter to form a double input converter. Also, because PCSC is considered as a current source, it can be located in parallel with a voltage buffer (capacitor) branch or output of other converter to form a double input converter. In [22], a new converter for power and energy management between battery, SC, and electric motor in an electric vehicle is proposed. In this converter, instead of two separate inductors as energy storage element, a coupled inductor is used. It is claimed that utilization of coupled inductors lead to 22%–26% volume reduction in comparison with two separated inductors. However, volume of coupled inductors is more than one inductor. Also, regeneration of brake energy to battery and SC in this converter is possible. In [23], a multiinput converter with just one inductor is proposed which is able to distribute load power between input sources. Also, in this converter, transferring power between sources is possible. In [24], a new extendable single stage multiinput dc–dc/ac boost converter proposed by the author.

On the other hand, it is important in electric vehicles to have low-torque ripple. Torque ripple has direct relation to voltage harmonics in ac motors. One way to reduce voltage harmonics is using of multilevel inverters. To generate multilevel voltage by multilevel inverters, dc sources with different or equal voltage level is required. One way to generate several dc-link is usage of multioutput dc–dc converters. In [25] and [26], a single inductor multioutput dc–dc converter is proposed which can generate several different voltage levels in its outputs. The converter is controlled to regulate the output voltages at their desired values despite the load power variation or input voltage variation. In [27], a new control method is proposed which is provided satisfactory dynamic performance for multioutput buck converter. But the shortcoming of these converters is their single input source. In other words, in applications such as electric vehicles that several input energy sources like fuel cell and battery are employed, this converter is not utilizable. One way to solve this problem is using of multiinput multioutput converters.

In [28] and [29], a nonisolated multiinput multioutput converter is introduced which has just one inductor. Using of large number of switches is drawback of this converter which caused low efficiency. Impossibility of energy transferring between input sources is other disadvantage of the proposed converter.

In this paper, a new multiinput multioutput nonisolated converter based on combination of a multiinput and a multioutput converter is proposed. The proposed converter compared to similar cases has less number of elements. This converter can control power flow between sources with each other and load. Also, proposed converter has several outputs that each one can have different voltage level. This paper is organized as follows. The converter structure and operation modes are explained in Section II. The dynamic modeling of the proposed converter is given in Section III. Section IV describes the control system of the proposed converter. Sections V and VI represents the simulations and experimental results, respectively, and Section VII concludes this paper.

II. Converter Structure and Operation Modes

As mentioned in the Introduction, in [25], a multioutput converter is presented. The proposed converter is a single input converter. On the other hand, use of just one input energy source in electric vehicles cannot provide load requirements because the load is dynamic and its power has variation. Therfore, hybridization of different sources is essential. As mentioned in the Introduction, in [23], a nonisolated multiinput dc–dc converter for hybridization of energy sources is proposed which has just one inductor. In this paper, a nonisolated multiinput multioutput dc–dc converter based on the combination of these two converters is proposed. The structure of the proposed converter is presented in Fig. 1. As seen from the figure, the converter interfaces m input power sources $V_{\text{in}1}$,$V_{\text{in}2}$,$V_{\text{in}3,}\ldots,V_{inm}$ such that $V_{\text{in}1} < V_{\text{in}2} < V_{\text{in}3} \ldots < V_{inm}$. The proposed converter has just one inductor, n capacitors in its outputs and $m+n$ switches. The R_1, $R_2, R_3, \ldots, R_n$ are the load resistances, which can represent the equivalent power feeding a multilevel inverter. By proper switching of switches, control of power flow between input sources in addition to boost up input sources voltages is possible. Outputs are capable to have different or equal voltage level which is appropriate for a connection to a multilevel inverter. The proposed converter is suitable

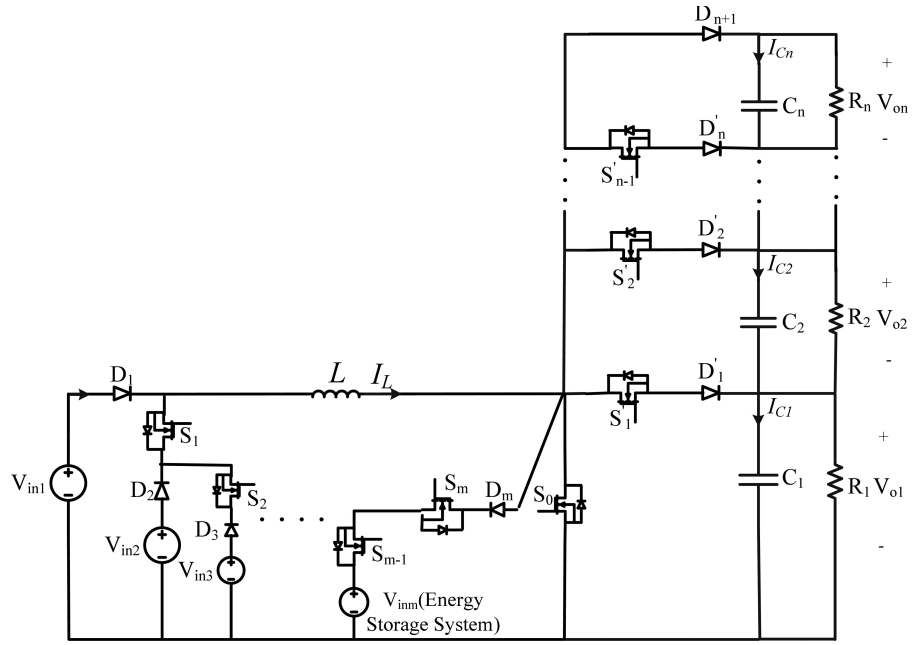

Fig. 1. Proposed converter structure.

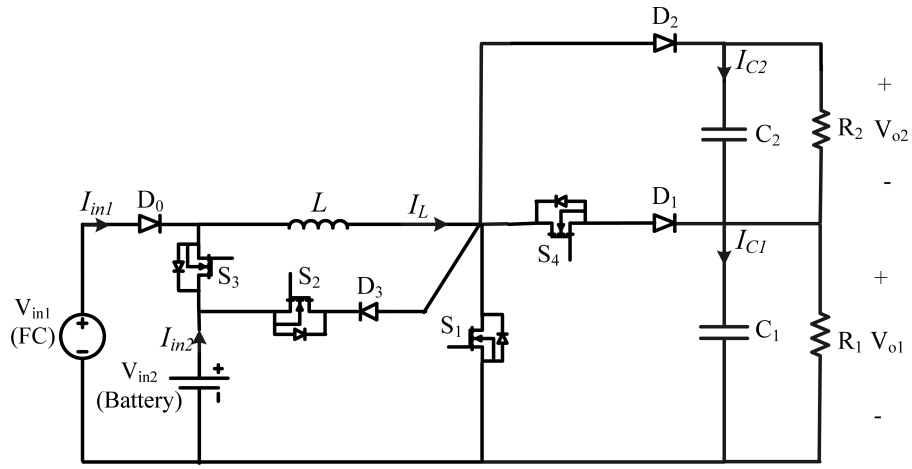

Fig. 2. Proposed converter with two-input, two-output.

alternative for hybridizing of FC, battery, or SC. In this paper, for convenience, proposed converter with two-input two-output is analyzed. In Fig. 2, the proposed converter with two-input two-output is shown. In this figure, R_1 and R_2 are the model of load resistances that can represent the equivalent power feeding a multilevel inverter. Different types of multilevel inverters can be used in connection to this converter. Multilevel inverter which is used must be with nonfloating dc-links. Four power switches S_1, S_2, S_3, and S_4 in the converter structure are the main controllable elements that control the power flow and output voltages of the converter. In the proposed converter, source $V_{\rm in1}$ can deliver power to source $V_{\rm in2}$ but not vice versa. So, in EV applications, FC which cannot be charged is located where $V_{\rm in1}$ is placed in circuit. Also, usually where $V_{\rm in2}$ is placed, ESSs such as battery or SC which are chargeable are located. In this paper, FC is used as a generating power source and the battery is used as an ESS. Depending on the utilization state of the battery, two power operation modes are defined for proposed converter. In each mode, just three of the four switches are active, while one switch is inactive. When load power is high, both input sources deliver power to load, in such a condition, S_2 is inactive and switches S_1, S_3, and S_4 are active. Also, when load power is low and $V_{\rm in2}$ is needed to be charged, $V_{\rm in1}$ not only supplies loads but also can charge $V_{\rm in2}$. In this condition, switches S_1, S_2, and S_4 are active and S_3 is inactive. In FCs, because of output voltage dependence to drawn current and also to make an exact power balance among the input powers and the load, ripple of drawn current should be minimized. Therefore, in this paper, steady state and dynamic behavior of the converter have been investigated in CCM. However, in battery charging

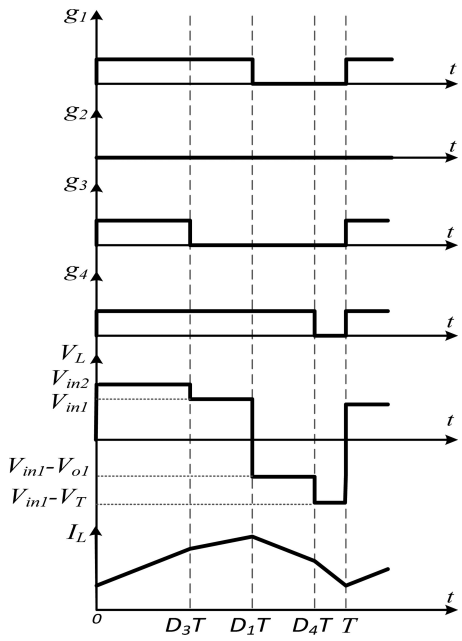

Fig. 3. Steady-state waveforms of proposed converter in battery discharging mode.

mode when the loads power and battery charging current have low values, it is possible that the converter works in discontinuous conduction mode (DCM). So, the condition in which the converter goes to DCM is investigated in Section III. It should be noted that each of input sources can be used separately. In other words, the converter can work as a single input dc–dc. Two main operation modes of the converter have been investigated as follows:

A. First Operation Mode (Battery Discharging Mode)

In this operation mode, two input power sources $V_{\rm in1}$ and $V_{\rm in2}\,(\rm battery)$ are responsible for supplying the loads. In this mode, S_2 is OFF entirely and S_1, S_3, and S_4 are active. For each switch, a specific duty is considered. Here, S_1 is active to regulate source 2 (battery) current to desired value. In fact, S_1 regulates battery current to desired value by controlling inductor current. Regulation of total output voltage $V_T = V_{O1} + V_{O2}$ to desired value is duty of the switch S_3. Also, output voltage V_{O1} is controlled by S_4. It is obvious that by regulation of V_T and V_{O1}, the output voltage V_{O2} is regulated too. Gate signals of switches and also voltage and current waveforms of inductor are shown in Fig. 3. According to switches states, there are four different operation modes in one switching period as follows:

1) Switching State 1 ($0 < t < D_3T$): In this state, switches S_1 and S_3 are turned ON. Because S_1 is ON, diodes D_1 and D_2 are reversely biased, so switch S_4 is turned OFF. Since S_3 is ON and $V_{\rm in1} < V_{\rm in2}$, diode D_0 is reversely biased. Equivalent circuit of proposed converter in this state is shown in Fig. 4(a). In this state, $V_{\rm in2}$ charges inductor L, so inductor current increases. Also, in this mode, capacitors C_1 and C_2 are discharged and deliver their stored energy to load resistances R_1 and R_2, respectively.

The inductor and capacitors equations in this mode are as follows:

$$\begin{cases} L\dfrac{di_L}{dt} = v_{\rm in2} \\ C_1\dfrac{dv_{O1}}{dt} = -\dfrac{v_{O1}}{R_1} \\ C_2\dfrac{dv_{O2}}{dt} = -\dfrac{v_{O2}}{R_2} \end{cases} \tag{1}$$

2) Switching State 2 ($D_3\,T < t < D_1\,T$): In this state, switch S_1 is still ON and S_3 is turned OFF. Because S_1 is ON, diodes D_1 and D_2 is reversely biased, so switch S_4 is still OFF. Equivalent circuit of proposed converter in this state is shown in Fig. 4(b). In this state, $V_{\rm in1}$ charges inductor L, so inductor current increases. In addition, capacitors C_1 and C_2 are discharged and deliver their stored energy to load resistances R_1 and R_2, respectively. The inductor and capacitors equations in this mode are as follows:

$$\begin{cases} L\dfrac{di_L}{dt} = v_{\rm in1} \\ C_1\dfrac{dv_{O1}}{dt} = -\dfrac{v_{O1}}{R_1} \\ C_2\dfrac{dv_{O2}}{dt} = -\dfrac{v_{O2}}{R_2}. \end{cases} \tag{2}$$

3) Switching State 3 ($D_1T < t < D_4T$): In this mode, switch S_1 is turned OFF and switch S_3 is still OFF. Also, switch S_4 is turned ON. Diode D_2 is reversely biased. Equivalent circuit of proposed converter in this state is shown in Fig. 4(c). In this state, inductor L is discharged and delivers its stored energy to C_1 and R_1, so inductor current is decreased. In this state, C_1 is charged and C_2 is discharged and delivers its stored energy to load resistance R_2. The energy storage elements L, C_1, and C_2 equations in this mode are as follows:

$$\begin{cases} L\dfrac{di_L}{dt} = v_{in1} - v_{O1} \\ C_1\dfrac{dv_{O1}}{dt} = i_L - \dfrac{v_{O1}}{R_1} \\ C_2\dfrac{dv_{O2}}{dt} = -\dfrac{v_{O2}}{R_2}. \end{cases} \tag{3}$$

4) Switching State 4 ($D_4T < t < T$): In this mode, all of three switches are OFF. So, diode D_2 is forward biased. In this state, inductor L is discharged and delivers its stored energy to capacitors C_1, C_2, and load resistances R_1 and R_2. Also, in this mode, capacitors C_1 and C_2 are charged. Equivalent circuit of proposed converter in this state is shown in Fig. 4(d). The inductor and capacitors equations in this mode are as follows:

$$\begin{cases} L\dfrac{di_L}{dt} = v_{\rm in1} - (v_{O1} + v_{O2}) \\ C_1\dfrac{dv_{O1}}{dt} = i_L - \dfrac{v_{O1}}{R_1} \\ C_2\dfrac{dv_{O2}}{dt} = i_L - \dfrac{v_{O2}}{R_2}. \end{cases} \tag{4}$$

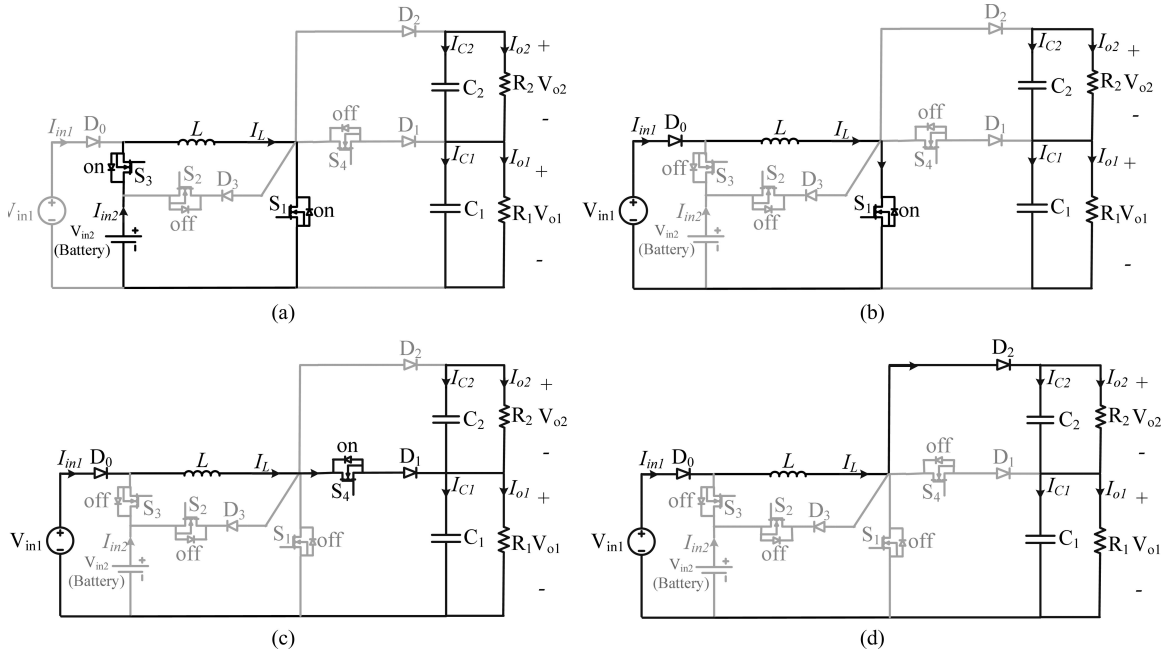

Fig. 4. Equivalent circuit of battery discharging mode, (a) switching state 1, (b) switching state 2, (c) switching state 3, (d) switching state 4.

B. Second Operation Mode (Battery Charging Mode)

In this mode, $V_{\rm in1}$ not only supplies loads but also delivers power to $V_{\rm in2}$ (battery). This condition occurs when load power is low and battery requires to be charged. In this operation mode, switches S_1, S_2, and S_4 are active and switch S_3 is entirely OFF. Like previous operation mode of the converter in this mode, for each switch, a specific duty is considered. S_1 is switched to regulate total output voltage $V_T = V_{O1} + V_{O2}$ to desired value. Regulation of the battery charging current (I_b) to desired value is the duty of switch S_2. Also, output voltage V_{O1} is controlled by switch S_4. It is clear that by regulation of V_T and V_{O1}, the output voltage V_{O2} is regulated too. In Fig. 5, gate signals of switches and voltage and current waveforms of inductor are shown. According to different switches states, there are four different operation modes in one switching period which is discussed as follows:

1) Switching State 1 ($0 < t < D_1T$): In this state, switch S_1 is turned ON, so S_2 and S_4 are reverse biased and cannot be turned ON. Also, diode D_2 is reversely biased and does not conduct. Equivalent circuit of proposed converter in this state is shown in Fig. 6(a). In this state, $V_{\rm in1}$ charges inductor L, so inductor current is increased. Also, in this mode, capacitors C_1 and C_2 are discharged and deliver their stored energy to load resistances R_1 and R_2, respectively. The inductor and capacitors equations in this mode are as follows:

$$\begin{cases} L\dfrac{di_L}{dt} = v_{\rm in1} \\ C_1\dfrac{dv_{O1}}{dt} = -\dfrac{v_{O1}}{R_1} \\ C_2\dfrac{dv_{O2}}{dt} = -\dfrac{v_{O2}}{R_2} \end{cases}. \tag{5}$$

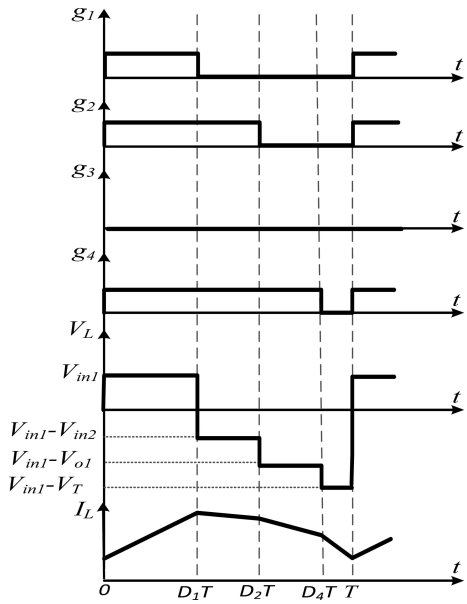

Fig. 5. Steady-state waveforms of proposed converter in battery charging mode.

2) Switching State 2 ($D_1T < t < D_2T$): In this mode, switch S_1 is turned OFF and switch S_2 is turned ON. Diode D_1 and D_2 are reversely biased, consequently, S_4 is still OFF. Equivalent circuit of proposed converter in this state is shown in Fig. 6(b). Since $V_{\rm in1} < V_{\rm in2}$, therefore, in this period of time, inductor current decreases and inductor delivers its stored energy to battery ($V_{\rm in2}$). Also, in this mode, capacitors C_1 and C_2 are discharged and deliver their stored energy to load resistances R_1 and R_2 respectively. The inductor and capacitors equations

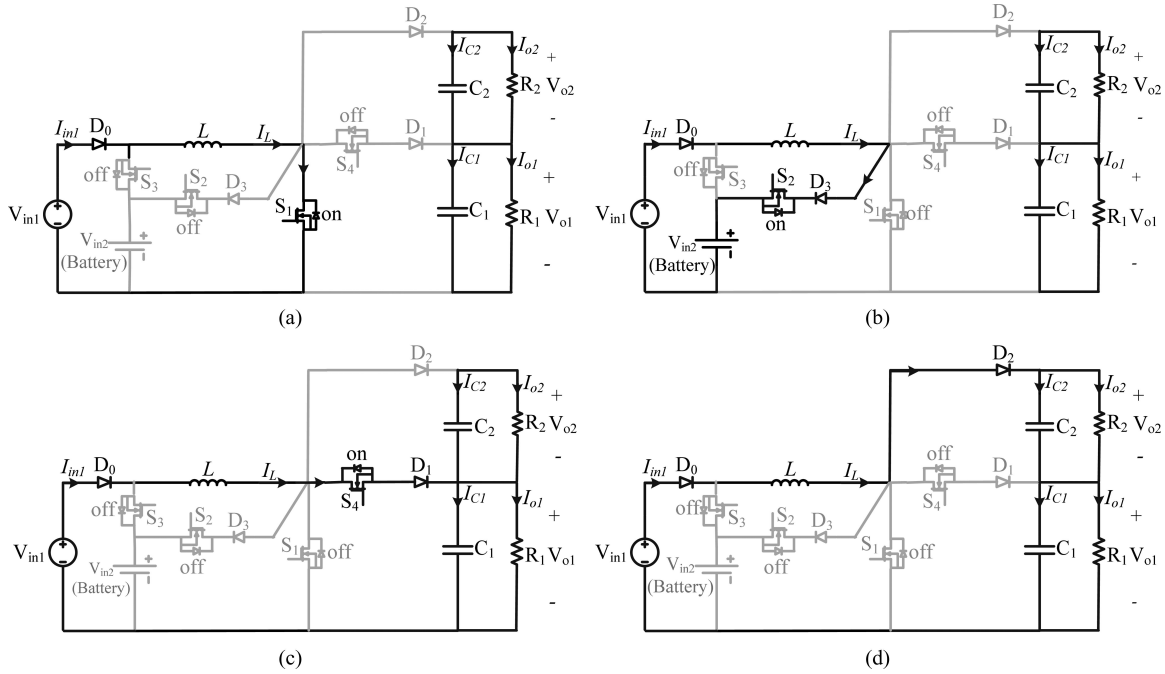

Fig. 6. Battery charging mode, (a) switching state 1, (b) switching state 2, (c) switching state 3, (d) switching state 4.

in this mode are as follows:

$$\begin{cases} L\dfrac{di_L}{dt} = v_{\text{in1}} - v_{\text{in2}} \\ C_1\dfrac{dv_{O1}}{dt} = -\dfrac{v_{O1}}{R_1} \\ C_2\dfrac{dv_{O2}}{dt} = -\dfrac{v_{O2}}{R_2} \end{cases}. \tag{6}$$

3) Switching State 3 ($D_2T < t < D_4T$): In this mode, switch S_1 is still OFF and switch S_2 is turned OFF and switch S_4 is turned ON. Also, diode D_2 is reversely biased. In Fig. 6(c), equivalent circuit of proposed converter in this state is shown. In this state, inductor L is discharged and delivers its stored energy to C_1 and R_1, so inductor current is decreased. In this state, capacitors C_1 is charged and capacitor C_2 is discharged and delivers its stored energy to load resistance R_2. The energy storage elements L, C_1, and C_2 equations in this mode are as follows:

$$\begin{cases} L\dfrac{di_L}{dt} = v_{\text{in1}} - v_{O1} \\ C_1\dfrac{dv_{O1}}{dt} = i_L - \dfrac{v_{O1}}{R_1} \\ C_2\dfrac{dv_{O2}}{dt} = -\dfrac{v_{O2}}{R_2} \end{cases}. \tag{7}$$

4) Switching State 4 ($D_4T < t < T$): In this mode, all the three switches are OFF. Therefore, diode D_2 is forward biased. In Fig. 6(d), an equivalent circuit of the proposed converter in this state is shown. In this state, inductor L is discharged and delivers its stored energy to capacitors C_1, C_2, and load resistances R_1 and R_2. Also, in this mode, capacitors C_1 and C_2 are charged. The inductor and capacitors equations in this mode are as follows:

$$\begin{cases} L\dfrac{di_L}{dt} = v_{\text{in1}} - (v_{O1} + v_{O2}) \\ C_1\dfrac{dv_{O1}}{dt} = i_L - \dfrac{v_{O1}}{R_1} \\ C_2\dfrac{dv_{O2}}{dt} = i_L - \dfrac{v_{O2}}{R_2} \end{cases}. \tag{8}$$

III. Dynamic Modeling Of the Proposed Converter

As mentioned in pervious section, the proposed converter is controlled by switches S_1, S_2, S_3, and S_4. Each switch has its own specific duty. By proper regulation of switches duty cycles, output voltages and battery charging or discharging current are adjustable. To design the closed loop controller for the converter, first dynamic model must be obtained. As stated in previous section, proposed converter has two main operation modes which in battery discharging mode two input sources deliver power to load and in battery charging mode, source V_{in1} not only supplies the load power but also charges V_{in2}(battery). There are different dynamic models for each operation modes of converter. Consequently, for both operation modes, different controller need to be designed separately.

A. Dynamic Model of Battery Discharging Mode

Small-signal model is the basis for optimized controller design. Especially, for such a multiinput multioutput converter, an effective model will be helpful to realize closed-loop control, and furthermore, to optimize the converter dynamics. Unlike

conventional single input single output converter, the multiport converter is a high-order system, and the symbolic derivation of these plant transfer functions is fairly tedious; therefore, it is difficult to obtain values of poles and zeros for analysis. Alternatively, the dynamics of the plant can be described in a matrix form; therefore, computer software is used to plot the bode graph of different transfer functions. Based on small-signal modeling method [30], the state variables, duty ratios, and input voltages contain two components, dc values (X, D, V) and perturbations ($\hat{x}$, $\hat{d}$, $\hat{v}$). It is assumed that the perturbations are small and do not vary significantly during one switching period. So, there are following equation for proposed converter:

$$\begin{cases} i_L(t) = I_L + \hat{i}_L(t) \\ v_{O1}(t) = V_{O1} + \hat{v}_{O1}(t) \\ v_{O2}(t) = V_{O2} + \hat{v}_{O2}(t) \\ d_1(t) = D_1 + \hat{d}_1(t) \\ d_2(t) = D_2 + \hat{d}_2(t) \\ d_3(t) = D_3 + \hat{d}_3(t) \\ d_4(t) = D_4 + \hat{d}_4(t) \end{cases} \tag{9}$$

where inductor current $i_L(t)$ and capacitor voltages $v_{O1}(t)$ and $v_{O2}(t)$ are state variables. If we substitute (9) into (1)–(4), apply the averaging to four state equations multiplied with corresponding duty cycle value, and then, neglect second-order terms, we obtain small-signal equations that are demonstrated as follows:

$$\begin{cases} L\frac{d\hat{i}_L(t)}{dt} = (V_{\text{in}2} - V_{\text{in}1})\,\hat{d}_3(t) + D_3\hat{v}_{\text{in}2}(t) \\ \qquad + (1 - D_3)\,\hat{v}_{\text{in}1}(t) \\ -(1 - D_1)\,\hat{v}_{O1}(t) + (D_4 - 1)\,\hat{v}_{O2}(t) \\ \qquad + V_{O1}\hat{d}_1(t) + V_{O2}\hat{d}_4(t) \\ C_1\frac{d\hat{v}_{O1}(t)}{dt} = -I_L\hat{d}_1(t) + (1 - D_1)\,\hat{i}_L(t) - \frac{\hat{v}_{O1}(t)}{R_1} \\ C_2\frac{d\hat{v}_{O2}(t)}{dt} = -I_L\hat{d}_4(t) + (1 - D_4)\,\hat{i}_L(t) - \frac{\hat{v}_{O2}(t)}{R_2} \end{cases}. \tag{10}$$

Therefore, the system can be represented in a matrix form using a state-space model such that $i_L(t)$, $v_{O1}(t)$, and $v_{O2}(t)$ are state variables. The state-space model takes the following form:

$$\begin{cases} \dfrac{dX}{dt} = AX + BU \\ Y = CX + DU \end{cases} \tag{11}$$

where X is a matrix containing the state variables, U is a matrix containing the control inputs $d_1(t)$, $d_3(t)$ and $d_4(t)$, and Y is a matrix containing the system outputs $v_{O1}(t)$, $v_T(t)$, and $i_b(t)$. So, matrixes X, Y, U take following form:

$$X = \begin{bmatrix} \hat{i}_L(t) \\ \hat{v}_{O1}(t) \\ \hat{v}_{O2}(t) \end{bmatrix},\ Y = \begin{bmatrix} \hat{v}_{O1}(t) \\ \hat{v}_T(t) \\ \hat{i}_b(t) \end{bmatrix},\ U = \begin{bmatrix} \hat{d}_4(t) \\ d_3(t) \\ \hat{d}_1(t) \end{bmatrix}. \tag{12}$$

Filling in the A, B, C, *and* D matrices using (10) and state equations (11), gives the following result:

$$A = \begin{bmatrix} 0 & \dfrac{(D_1 - 1)}{L} & \dfrac{(D_4 - 1)}{L} \\ \dfrac{(1 - D_1)}{C_1} & -\dfrac{1}{R_1C_1} & 0 \\ \dfrac{(1 - D_4)}{C_2} & 0 & -\dfrac{1}{R_2C_2} \end{bmatrix}$$

$$B = \begin{bmatrix} \dfrac{V_{O2}}{L} & \dfrac{V_{O1}}{L} & \dfrac{V_{\text{in}2} - V_{\text{in}1}}{L} \\ 0 & -\dfrac{I_L}{C_1} & 0 \\ -\dfrac{I_L}{C_2} & 0 & 0 \end{bmatrix}$$

$$C = \begin{bmatrix} 0 & 1 & 0 \\ 0 & 1 & 1 \\ D_3 & 0 & 0 \end{bmatrix},\ D = \begin{bmatrix} 0 & 0 & 0 \\ 0 & 0 & 0 \\ 0 & I_L & 0 \end{bmatrix} \tag{13}$$

where $V_{\text{in}1}$ and $V_{\text{in}2}$ are input sources voltages. Also, V_{O1} and V_{O2} are output voltages. In the$A$, B, C, *and* D matrices, all parameters except duty cycle of switches D_1, D_3, D_4, and dc value of inductor current I_L, are known. For the inductor current, there is the following equation:

$$I_L = \frac{I_b}{D_3} \tag{14}$$

where I_b is the battery current. So, the only unknown parameters of expressed matrices are D_1, D_3, and D_4. The values of switches duty cycles are obtained by steady-state equations which expressed in following equation:

$$\begin{bmatrix} V_{O1} & V_{\text{in}2} - V_{\text{in}1} & V_{O2} \\ R_1I_b & V_{O1} & 0 \\ 0 & V_{O2} & R_2I_b \end{bmatrix} \begin{bmatrix} D_1 \\ D_3 \\ D_4 \end{bmatrix} = \begin{bmatrix} V_{O2} + V_{O1} - V_{\text{in}1} \\ R_1I_b \\ R_2I_b \end{bmatrix}. \tag{15}$$

So, from the aforementioned matrix equation, duty cycles of switches achieved and are placed in $A, B, C,$ *and* D matrices. As represented in the system small-signal models, state variables are controlled by three control variables $d_1(t)$, $d_3(t)$, and $d_4(t)$. The transfer function matrix of the converter is obtained from the small signal model as follows:

$$G = C\,(SI - A)^{-1}\,B + D \tag{16}$$

where

$$y = Gu. \tag{17}$$

The rank of transfer function matrix denotes the number of control variables. In this paper, according to the number of control variables and based on (12), rank of transfer function matrix G is 3×3

$$\underbrace{\begin{bmatrix} y_1 \\ y_2 \\ y_3 \end{bmatrix}}_{y} = \underbrace{\begin{bmatrix} g_{11} & g_{12} & g_{13} \\ g_{21} & g_{22} & g_{23} \\ g_{31} & g_{32} & g_{33} \end{bmatrix}}_{G} \underbrace{\begin{bmatrix} u_1 \\ u_2 \\ u_3 \end{bmatrix}}_{u} \tag{18}$$

where y and u are the system output and input vectors, and component g_{ij} represents the transfer function between y_i and u_j. So, there are three transfer functions as follows:

$$\begin{cases} \dfrac{\hat{v}_{O1}(s)}{\hat{d}_4(s)} = g_{11} \\ \dfrac{\hat{v}_T(s)}{\hat{d}_3(s)} = g_{22} \\ \dfrac{\hat{i}_b(s)}{\hat{d}_1(s)} = g_{33} \end{cases}. \tag{19}$$

B. Dynamic Model of Battery Charging Mode

In this operation mode of proposed converter, which $V_{\text{in}1}$ delivers energy to loads and $V_{\text{in}2}$ (battery), switches S_1, S_2, and S_4 are active and switch S_3 is inactive. Like battery discharging mode, first small signal model should be obtained by substituting (9) into (5)–(8), apply the averaging to four state equations multiplied with corresponding duty cycle value, and then, neglect second-order terms, we obtain small-signal equations that are demonstrated as follows:

$$\begin{cases} L\frac{d\hat{i}_L(t)}{dt} = \hat{v}_{\text{in}1}(t) + V_{\text{in}2}\hat{d}_1(t) + (D_1 - D_2)\,\hat{v}_{\text{in}2}(t) \\ + (V_{O1} - V_{\text{in}2})\,\hat{d}_2(t) + V_{O2}\hat{d}_4(t) + (D_2 - 1)\,\hat{v}_{O1}(t) \\ \quad - (1 - D_4)\,\hat{v}_{O2}(t) \\ C_1\frac{d\hat{v}_{O1}(t)}{dt} = -I_L\hat{d}_2(t) + (1 - D_2)\,\hat{i}_L(t) - \frac{\hat{v}_{O1}(t)}{R_1} \\ C_2\frac{d\hat{v}_{O2}(t)}{dt} = -I_L\hat{d}_4(t) + (1 - D_4)\,\hat{i}_L(t) - \frac{\hat{v}_{O2}(t)}{R_2} \end{cases}. \tag{20}$$

These equations can be expressed as state space equations. In this operation mode similar to battery discharging mode $i_L(t)$, $v_{O1}(t)$, and $v_{O2}(t)$ are the state variables. State variables, input, and output matrices are illustrated as follows:

$$y = \begin{bmatrix} \hat{v}_{O1}(t) \\ \hat{v}_T(t) \\ \hat{i}_b(t) \end{bmatrix} \quad X = \begin{bmatrix} \hat{i}_L(t) \\ \hat{v}_{O1}(t) \\ \hat{v}_{O2}(t) \end{bmatrix} \quad u = \begin{bmatrix} \hat{d}_4(t) \\ \hat{d}_1(t) \\ \hat{d}_2(t) \end{bmatrix} \tag{21}$$

where $v_T(t) = v_{O1}(t) + v_{O2}(t)$. Finally for this operation mode of converter, similar to pervious mode, there are A, B, C, *and* D matrices as follows:

$$A = \begin{bmatrix} 0 & \frac{(D_2-1)}{L} & \frac{(D_4-1)}{L} \\ \frac{(1-D_2)}{C_1} & -\frac{1}{R_1C_1} & 0 \\ \frac{(1-D_4)}{C_2} & 0 & -\frac{1}{R_2C_2} \end{bmatrix}$$

$$B = \begin{bmatrix} \frac{V_{\text{in}2}}{L} & \frac{(V_{O1}-V_{\text{in}2})}{L} & \frac{V_{O2}}{L} \\ 0 & -\frac{I_L}{C_1} & 0 \\ 0 & 0 & -\frac{I_L}{C_2} \end{bmatrix}$$

$$C = \begin{bmatrix} 0 & 1 & 0 \\ 0 & 1 & 1 \\ D_2 - D_1 & 0 & 0 \end{bmatrix} \quad D = \begin{bmatrix} 0 & 0 & 0 \\ 0 & 0 & 0 \\ -I_L & I_L. & 0 \end{bmatrix} \tag{22}$$

In the aforementioned matrices, all parameters except duty cycle of switches D_1, D_2, D_4, and dc value of inductor current I_L are known. For the inductor current, there is following equation:

$$I_L = \frac{I_b}{D_2 - D_1} \tag{23}$$

where I_b is desired value of battery current. So, the unknown parameters of expressed matrices are D_1, D_2, and D_4. The values of switches duty cycle are obtained by steady-state equations

$$\begin{bmatrix} V_{\text{in}2} & V_{O1} - V_{\text{in}2} & V_{O2} \\ -V_{O1} & V_{O1} + R_1I_b & 0 \\ -V_{O2} & V_{O2} & R_2I_b \end{bmatrix} \begin{bmatrix} D_1 \\ D_2 \\ D_4 \end{bmatrix} = \begin{bmatrix} V_{O1} + V_{O2} - V_{\text{in}1} \\ R_1I_b \\ R_2I_b \end{bmatrix}. \tag{24}$$

The transfer function matrix of the converter is obtained from the small signal model as follows:

$$G = C\,(SI - A)^{-1}\,B + D \tag{25}$$

where

$$y = Gu \tag{26}$$

where y and u are the system output and input vectors, so the three transfer functions are as follows:

$$\begin{cases} \dfrac{\hat{v}_{O1}(s)}{\hat{d}_4(s)} = g_{11} \\ \dfrac{\hat{v}_T(s)}{\hat{d}_1(s)} = g_{22} \\ \dfrac{\hat{i}_b(s)}{\hat{d}_2(s)} = g_{33} \end{cases}. \tag{27}$$

Also, it is noteworthy that in battery charging mode when the loads power and battery current have low values, it is possible that the converter goes to discontinuous conduction mode. It is known that dc–dc converters will work in DCM if their inductor dc current be less than their inductor current ripple. So, for the proposed converter in battery charging mode by averaging of the inductor voltage and capacitors current during a switching period, the dc equations can be obtained as follows:

$$\begin{cases} V_{\text{in}2}D_1 + (V_{O1} - V_{\text{in}2})\,D_2 + V_{O2}D_4 \\ \quad = V_{O1} + V_{O2} - V_{\text{in}1} \\ -I_LD_2 + I_L = \frac{V_{O1}}{R_1} \\ -I_LD_4 + I_L = \frac{V_{O2}}{R_2} \end{cases} \tag{28}$$

also, the inductor current ripple in battery charging mode can be expressed as

$$\Delta I_L = \frac{V_{\text{in}1}D_1T_s}{L}. \tag{29}$$

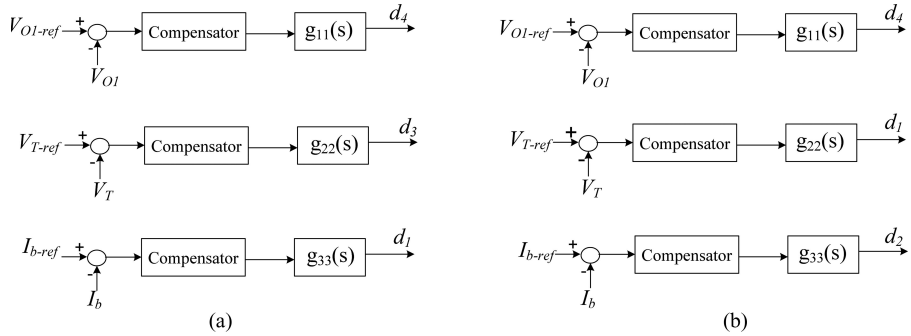

Fig. 7. Control block diagram of proposed converter (a) battery discharging mode, (b) battery charging mode.

So, from (23), (28), and (29), the converter will work in DCM if the following conditions be satisfied:

$$\begin{cases} I_L = \dfrac{V_{O1}}{R_1(1-D_2)} < \dfrac{V_{\text{in}1} D_1 T_s}{L} \\ I_L = \dfrac{V_{O2}}{R_2(1-D_4)} < \dfrac{V_{\text{in}1} D_1 T_s}{L} \\ I_L = \dfrac{I_b}{(D_2-D_1)} < \dfrac{V_{\text{in}1} D_1 T_s}{L} \end{cases} \tag{30}$$

which (30) can be rewritten as

$$\begin{cases} R_1 > \dfrac{V_{O1} L f_s}{D_1(1-D_2)V_{\text{in}1}} \\ R_2 > \dfrac{V_{O2} L f_s}{D_1(1-D_4)V_{\text{in}1}} \\ I_b < \dfrac{V_{\text{in}1} D_1 (D_2-D_1)}{L f_s} \end{cases}. \tag{31}$$

In fact, (31) confirms this fact that the proposed converter will work in DCM when the output loads are light and the battery charging current has low value.

IV. Controller Design

Transfer functions of two operation modes of the converter derived in previous section. As transfer functions in two operation modes of converter are different, consequently, for each mode, different controller is needed to be designed separately. In Fig. 7, control block diagrams of converter in two operation mode are shown. In battery discharging mode $R_1 = R_2 = 35\,\Omega$ and in battery charging mode $R_1 = R_2 = 70\,\Omega$.

A. Controller Design for Battery Discharging Mode

As discussed in Section III, in this mode, we have three transfer functions. For each transfer function, frequency-domain bode plot analysis need to be obtained by computer software to design the system compensators. System compensators should provide desired steady-state error and sufficient phase margin, high stability, and high bandwidth. Utilizing A, B, C, *and* D matrices which are illustrated in section III and transfer function matrix G, transfer function of g_{11} is (32) shown at the bottom of the page.

TABLE I
Simulation and Prototype Parameters

Simulation & Prototype parameters	Symbols
2.5 mH	L
1000 μF	C_1
1000 μF	C_2
35 Vs	$V_{\text{in}1}$
48 V	V_{Battery} ($V_{\text{in}2}$)
10 kHz	f_s

Using MATLAB software, the open loop bode diagram of g_{11} for converter simulation parameters which is shown in table I is achieved. Bode diagrams are shown in Fig. 8(a). Investigating the obtained bode plots, it can be understood that in crossover frequency phase of g_{11} is –179.99°. So, the phase margin is not sufficient and closed loop system is unstable. Consequently, to increase phase margin and improve system stability, a lead compensator is designed

$$K(S) = K\frac{S+Z}{S+P} \tag{33}$$

where in this equation $K = 2.9$, $Z = 906.05$, and $P = 7641.6$. In Fig. 8(b), bode diagrams after compensation are shown. It is obvious that by utilizing lead compensator, stability of the system has been provided. Also, transfer function of g_{22} is (34), see at the bottom of the next page.

In Fig. 9(a), bode diagrams for g_{22} are shown. It can be found from bode diagrams that the phase margin of g_{22} is

$$g_{11} = \frac{\hat{v}_{O1}(s)}{\hat{d}_4(s)} = \frac{\left(\frac{V_{O2}(1-D_1)}{LC_1}\right)S + \left(\frac{(1-D_1)V_{O2}}{LR_2C_1C_2} - \frac{(1-D_1)(D_4-1)I_L}{LC_1C_2}\right)}{S^3 + \left(\frac{R_1C_1+R_2C_2}{R_1R_2C_1C_2}\right)S^2 + \left(\frac{L+(1-D_1)^2R_1R_2C_2+(D_4-1)^2R_1R_2C_1}{LR_1R_2C_1C_2}\right)S + \left(\frac{R_1(1-D_1)^2+(D_4-1)^2R_2}{LR_1R_2C_1C_2}\right)} \tag{32}$$

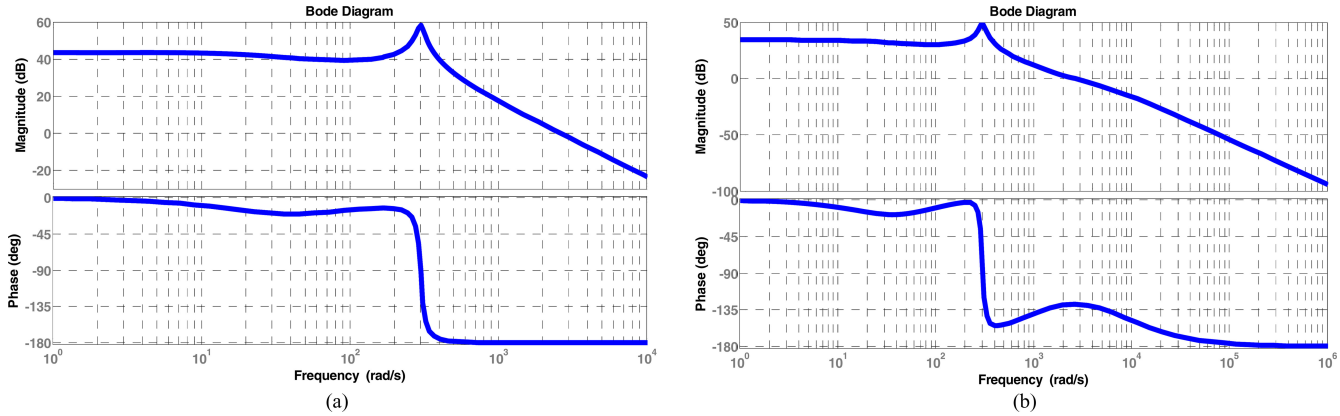

Fig. 8. Simulated Bode plots of $g_{11}(s)$. (a) Before applying the compensator. (b) After applying the compensator.

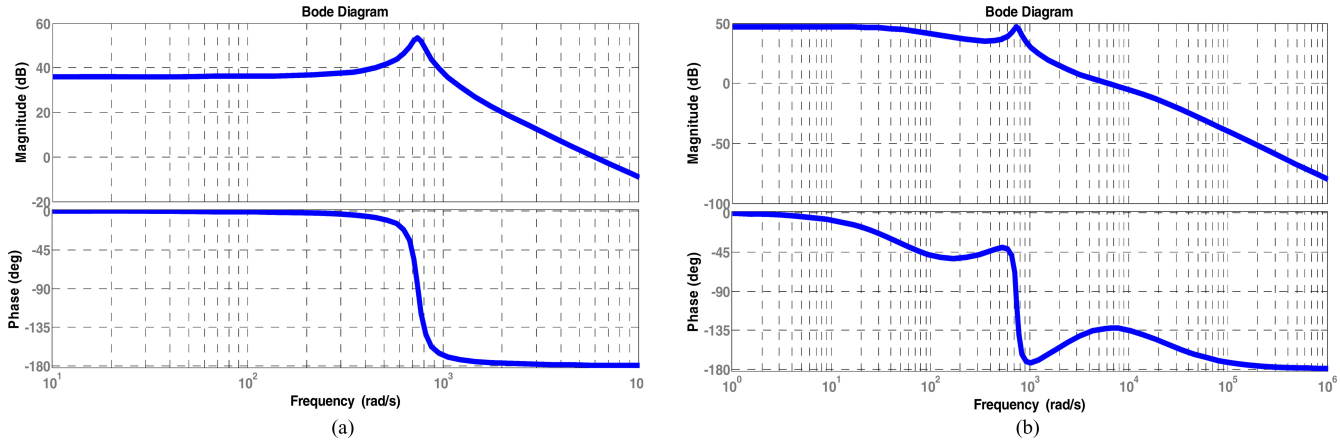

Fig. 9. Simulated Bode plots of $g_{22}(s)$. (a) Before applying the compensator. (b) After applying the compensator.

inadequate, so a lead compensator is required. Consequently, a lead compensator by following transfer function is employed:

$$K_{\text{lead}}(S) = 2.8960\frac{S+2098.9}{S+16982}. \tag{35}$$

But using of this lead compensator reduces dc gain and, consequently, leads to increase of steady state error. Conquering this problem, lag compensator is added to system. To avoid the effect of lag compensator on lead compensator, zero of lag compensator is determined ten times smaller than crossover frequency. So, the transfer function of lag is as follows:

$$K_{\text{lag}}(s) = K\frac{S+Z}{S+P} \tag{36}$$

where $K = 1$, Z= 583.45 and $P = 58.345$. In Fig. 9(b), bode diagrams after compensation by lead-lag compensators are shown.

As mentioned previously, the current of source 2 (battery) is controlled by switch S_1. In fact, S_1 controls the inductor current to set the battery current to desired value the related transfer function is shown in (37), at the bottom of the page.

$$g_{22} = \frac{\hat{v}_T(s)}{\hat{d}_3(s)} = \frac{\left(\frac{V_{\text{in}2}-V_{\text{in}1}}{L}\right)\left(\frac{(1-D_1)}{C_1} - \frac{(D_4-1)}{C_2}\right)S + \left(\frac{(1-D_1)}{R_2C_1C_2} - \frac{(D_4-1)}{R_1C_1C_2}\right)\left(\frac{V_{\text{in}2}-V_{\text{in}1}}{L}\right)}{S^3 + \left(\frac{R_1C_1+R_2C_2}{R_1R_2C_1C_2}\right)S^2 + \left(\frac{L+(1-D_1)^2R_1R_2C_2+(D_4-1)^2R_1R_2C_1}{LR_1R_2C_1C_2}\right)S + \left(\frac{R_1(1-D_1)^2+(D_4-1)^2R_2}{LR_1R_2C_1C_2}\right)} \tag{34}$$

$$g_{33} = \frac{\hat{i}_b(s)}{\hat{d}_1(s)} = \frac{\left(\frac{V_{O1}D_3}{L}\right)S^2 + \left(\frac{D_3V_{O1}}{L}\left(\frac{1}{R_1C_1}+\frac{1}{R_2C_2}\right) + \frac{I_L(1-D_1)D_3}{LC_1}\right)S + \left(\frac{D_3V_{O1}}{LR_1R_2C_1C_2} + \frac{I_L(1-D_1)D_3}{LR_2C_1C_2}\right)}{S^3 + \left(\frac{R_1C_1+R_2C_2}{R_1R_2C_1C_2}\right)S^2 + \left(\frac{L+(1-D_1)^2R_1R_2C_2+(D_4-1)^2R_1R_2C_1}{LR_1R_2C_1C_2}\right)S + \left(\frac{R_1(1-D_1)^2+(D_4-1)^2R_2}{LR_1R_2C_1C_2}\right)} \tag{37}$$

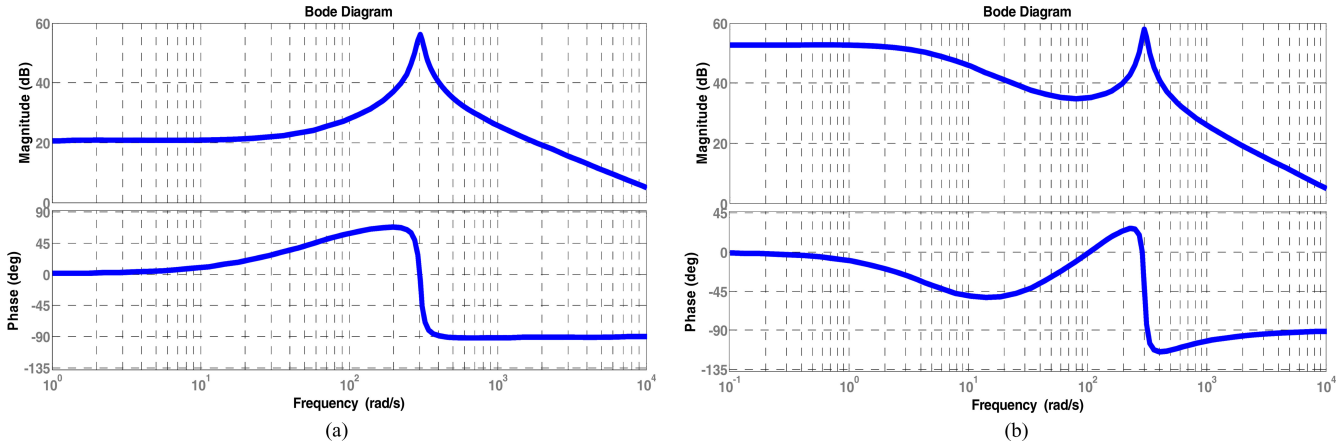

Fig. 10. Simulated Bode plots of $g_{33}(s)$. (a) Before applying the compensator. (b) After applying the compensator.

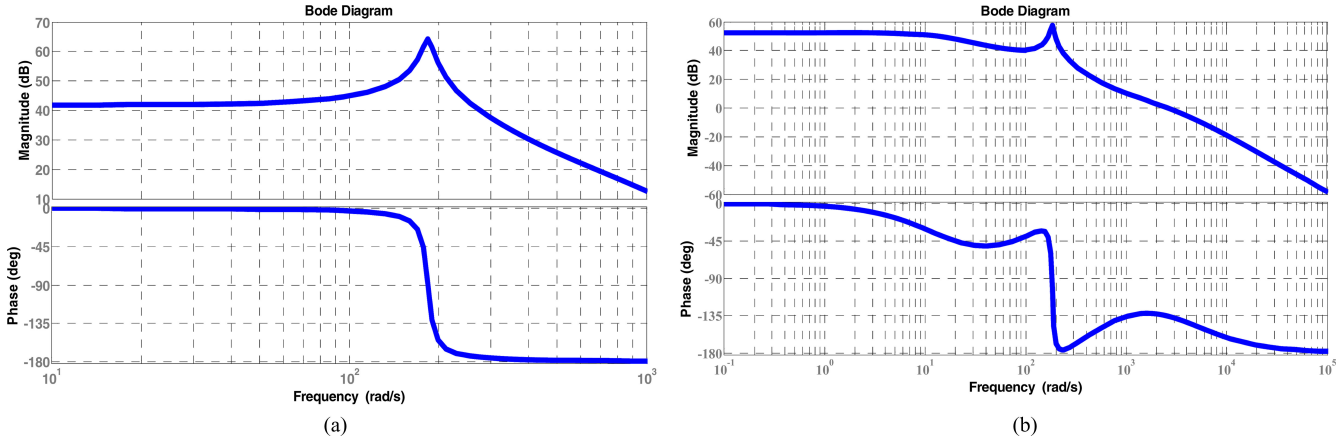

Fig. 11. Simulated Bode plots of $g_{11}(s)$. (a) Before applying the compensator. (b) After applying the compensator.

Bode diagram of g_{33} is shown in Fig. 10(a). As seen from figure, phase margin is adequate, as result system is stable but the dc gain is low. Consequently, steady-state error has significant value. To reduce steady-state error, a lag compensator is employed

$$K_{\text{lag}}(s) = \frac{S+200}{S+5}. \tag{38}$$

In Fig. 10(b), bode diagrams after applying lag compensator are shown.

B. Controller Design for Battery Charging Mode of the Converter

In this operation mode as cited in previous section, switches S_1, S_2, and S_4 are active and S_3 is inactive. In this mode, switch S_4 is used to regulate output voltage V_{O1}, the related transfer function is shown in (39), the bottom of the page.

Bode diagram of g_{11} is shown in Fig. 11(a). Because of insufficient phase margin, lead compensator is needed. So, lead compensator by following transfer function is designed:

$$K_{\text{lead}}(S) = 2.9\frac{S+482.7}{S+4065.8}. \tag{40}$$

To reduce steady-state error following lag compensator is added to system:

$$K_{\text{lag}}(S) = \frac{S+140}{S+14}. \tag{41}$$

In Fig. 11(b), bode diagram after applying lead-lag compensator is shown. Also, in this operation mode, switch S_1 is used to regulate total output voltage V_T, the related transfer function is shown in (42), at the bottom of the next page.

Bode diagram of g_{22} is shown in Fig. 12(a).

$$g_{11} = \frac{\hat{v}_{O1}(s)}{\hat{d}_4(s)} = \frac{\left(\frac{V_{O2}(1-D_2)}{LC_1}\right)S + \left(\frac{(1-D_2)V_{O2}}{LR_2C_1C_2} - \frac{(1-D_2)(D_4-1)I_L}{LC_1}\right)}{S^3 + \left(\frac{R_1C_1+R_2C_2}{R_1R_2C_1C_2}\right)S^2 + \left(\frac{L+(D_2-1)^2R_1R_2C_2+(D_4-1)^2R_1R_2C_1}{LR_1R_2C_1C_2}\right)S + \left(\frac{R_1(D_2-1)^2+(D_4-1)^2R_2}{LR_1R_2C_1C_2}\right)} \tag{39}$$

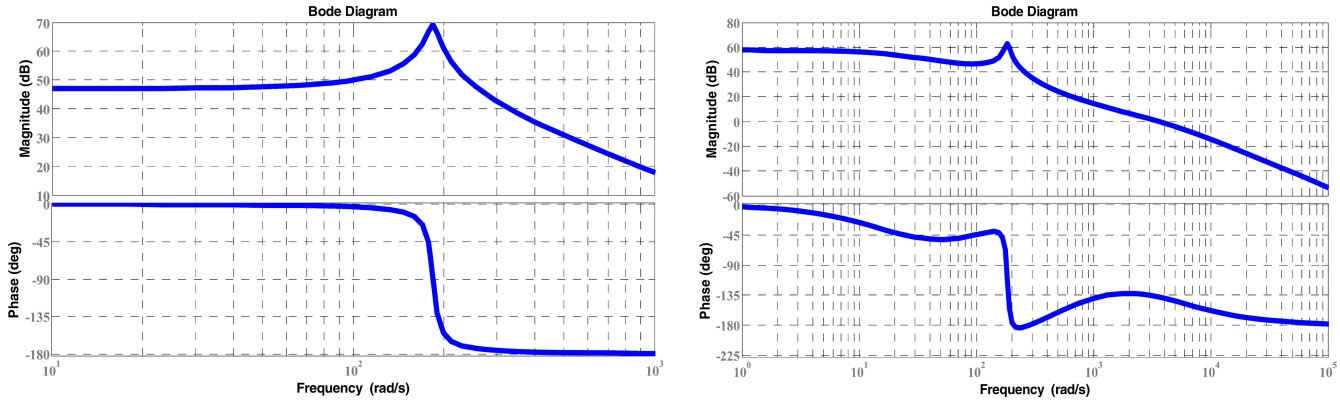

Fig. 12. Bode plots of g_{22}(s). (a) Before applying the compensator. (b) After applying the compensator.

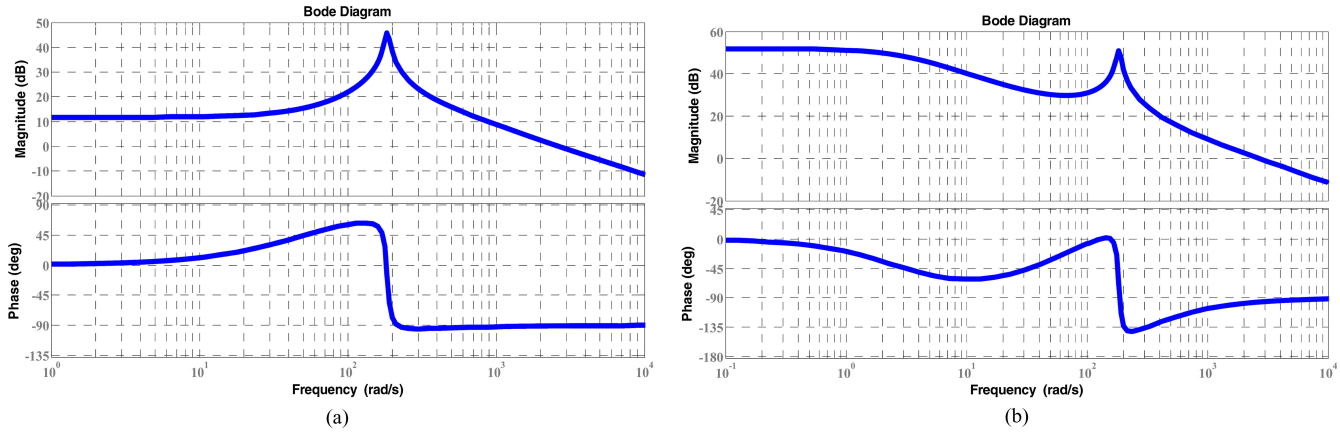

Fig. 13. Bode plots of g_{33}(s). (a) Before applying the compensator. (b) After applying the compensator.

Because of insufficient phase margin of g_{22}, following lead compensator is used:

$$K_{\text{lead}}(S) = 2.9\frac{S+585.4}{S+4937}. \tag{43}$$

Also, to reduce steady-state error following lag compensator is applied:

$$K_{\text{lag}}(S) = \frac{S+170}{S+17} \tag{44}$$

In Fig. 12(b), bode diagram after compensation is shown. Besides, switch S_2 for regulation of battery charging current is used the related transfer function is shown in (45), at the bottom of the page.

Bode diagram of g_{33} is shown in Fig. 13(a). It is obvious from figure that phase margin is sufficient, so there is no need for stabilizing compensator. Just a lag compensator for reducing of steady-state error is used

$$K_{\text{lag}}(S) = \frac{S+267.4}{S+2.67}. \tag{46}$$

$$g_{22} = \frac{\hat{v}_T(s)}{\hat{d}_1(s)} = \frac{\left(\frac{V_{\text{in}2}(1-D_2)}{LC_1} + \frac{(1-D_4)V_{\text{in}2}}{LC_2}\right)S + \left(\frac{(1-D_2)V_{\text{in}2}}{LR_2C_1C_2} + \frac{(1-D_4)V_{\text{in}2}}{LR_1C_1C_2}\right)}{S^3 + \left(\frac{R_1C_1+R_2C_2}{R_1R_2C_1C_2}\right)S^2 + \left(\frac{L+(D_2-1)^2R_1R_2C_2+(D_4-1)^2R_1R_2C_1}{LR_1R_2C_1C_2}\right)S + \left(\frac{R_1(D_2-1)^2+(D_4-1)^2R_2}{LR_1R_2C_1C_2}\right)} \tag{42}$$

$$g_{33} = \frac{\hat{i}_b(s)}{\hat{d}_2(s)}$$
$$= \frac{\frac{(D_2-D_1)(V_{O1}-V_{\text{in}2})}{L}S^2 + \left(\frac{(V_{O1}-V_{\text{in}2})(D_2-D_1)}{L}\left(\frac{1}{R_1C_1}+\frac{1}{R_2C_2}\right) - \frac{I_L(D_2-D_1)(D_2-1)}{LC_1}\right)S + \left(\frac{(D_2-D_1)(V_{O1}-V_{in2})}{LR_1R_2C_1C_2} - \frac{(D_2-1)(D_2-D_1)I_L}{LR_2C_1C_2} + I_L\right)}{S^3 + \left(\frac{R_1C_1+R_2C_2}{R_1R_2C_1C_2}\right)S^2 + \left(\frac{L+(D_2-1)^2R_1R_2C_2+(D_4-1)^2R_1R_2C_1}{LR_1R_2C_1C_2}\right)S + \left(\frac{R_1(D_2-1)^2+(D_4-1)^2R_2}{LR_1R_2C_1C_2}\right)} \tag{45}$$

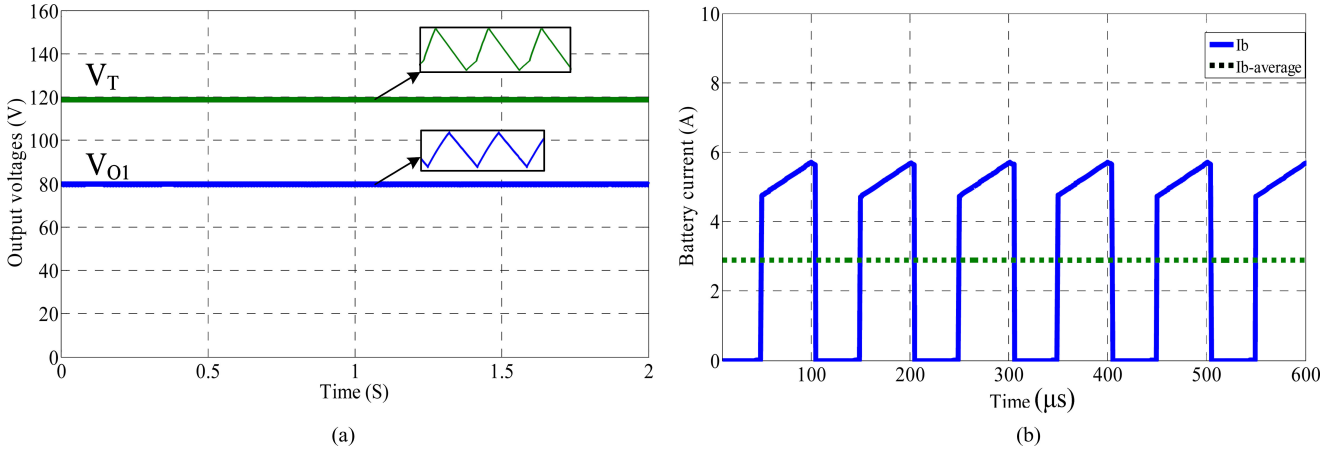

Fig. 14. Simulation results in battery discharging mode, (a) output voltages, (b) battery current.

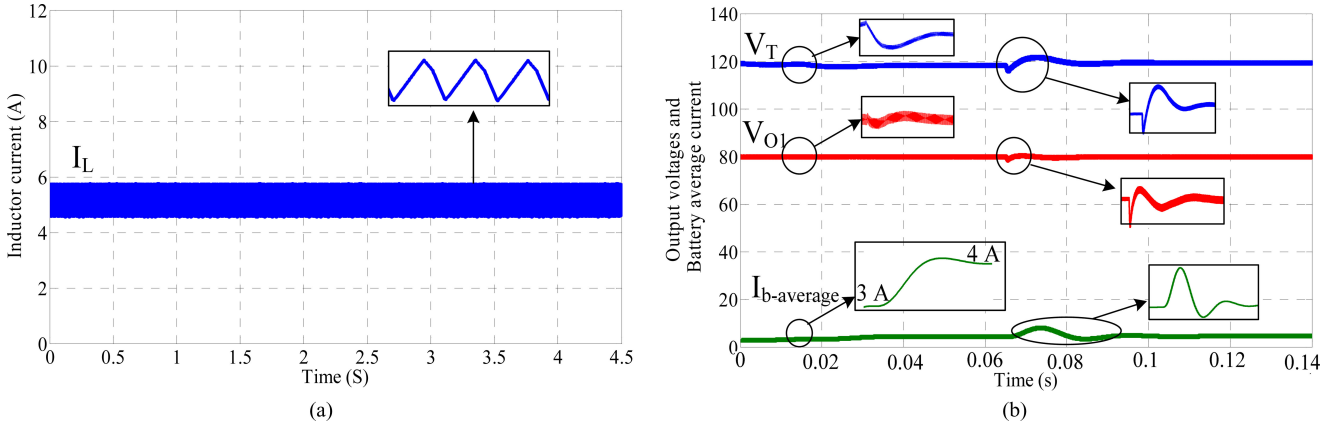

Fig. 15. Simulation results in battery discharging mode, (a) inductor current, (b) output voltages and battery current in changing battery reference current and load power increase condition.

In Fig. 13(b), bode diagram after compensation is shown.

V. Simulation Results

In order to verify the performance of the proposed converter, simulations have been done in battery discharging and charging modes by PSCAD/EMTDC software. The simulation parameters of the converter are listed in Table I. Input voltage sources are considered $V_{\text{in}1} = 35\,\text{V}$, $V_{\text{in}2} = 48\,\text{V}$. In simulations, battery model is used as input source 2. The output voltages of the converter are desired to be regulated on $V_{O1-\text{ref}} = 80\,\text{V}$ and $V_{O2-\text{ref}} = 40\,\text{V}$. Consequently, total output voltage is desired to be regulated on $V_{T-\text{ref}} = 120\,\text{V}$. Also, battery current is desired to be regulated on $I_{b-\text{ref}} = 3\,\text{A}$ and $I_{b-\text{ref}} = -0.9\,\text{A}$ for battery discharging and charging modes, respectively. Load resistances are $R_1 = R_2 = 35\,\Omega$ and $R_1 = R_2 = 70\,\Omega$ for battery discharging and charging modes, respectively. In the beginning, battery discharging mode of the converter is investigated. As mentioned in previous sections, in this mode switches S_1, S_3, and S_4 are active. Each switch is controlled by compensator which is designed in Section IV. In Fig. 14(a), output voltages V_{O1} and V_T are shown. As seen from this figure, the output voltages are regulated to the desired values. In Fig. 14(b), battery current is shown. It is clear that battery current is tracked the reference value well. In Fig. 15(a), inductor current is shown. At a particular time ($t \cong 0.01\,\text{s}$), the battery current reference is increased suddenly from 3 to 4 A. Also at specific time ($t \cong 0.07\,\text{s}$), the loads power are increased suddenly. At that time, load resistances are changed to $R_1 = R_2 = 17.5\,\Omega$. In Fig. 15(b), output voltages and battery current under these conditions are shown. As seen from this figure, controllers regulated output voltages and battery current against loads changes very well. In fact, by controlling battery current, distribution of load power between input sources is feasible. In battery charging mode, source 1 in addition to supply the loads delivers power to source 2 (battery). In this mode, switches S_1, S_2, and S_4 are active. In this mode, similar to battery discharging mode, desired values of output voltages are $V_{O1-\text{ref}} = 80\,\text{V}$, $V_{O2-\text{ref}} = 40\,\text{V}$, and battery charging current reference is $I_{b-\text{ref}} = -0.9\,\text{A}$. In this state, the compensators which are designed for battery charging mode of the converter are used. In Fig. 16(a), output voltages V_{O1} and V_{O2} are shown. As seen from this figure, the output voltages

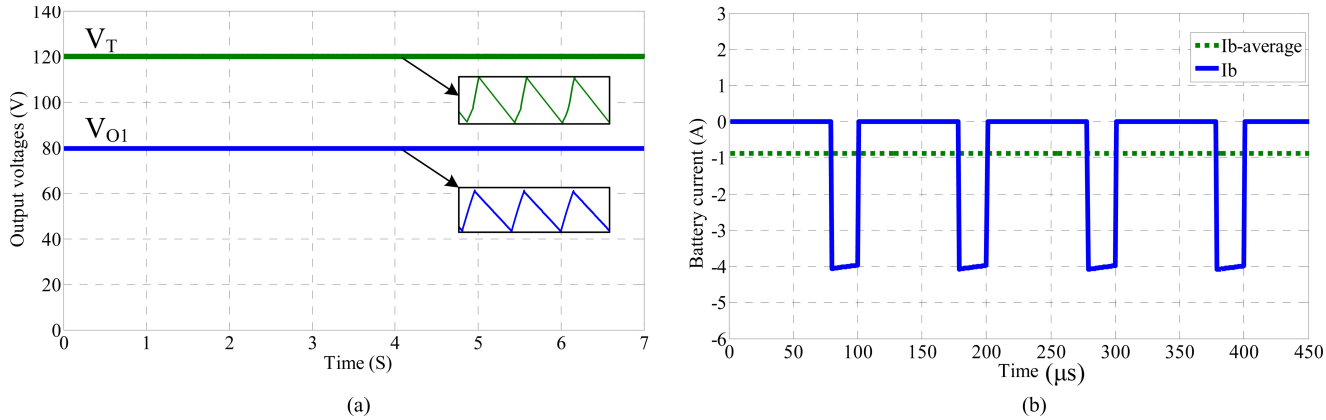

Fig. 16. Simulation results in battery charging mode, (a) output voltages, (b) battery current.

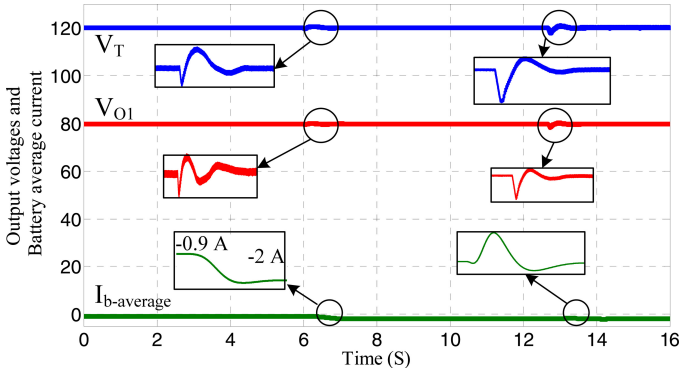

Fig. 17. Output voltages and battery current in increase of loads power and decrease of battery reference current conditions.

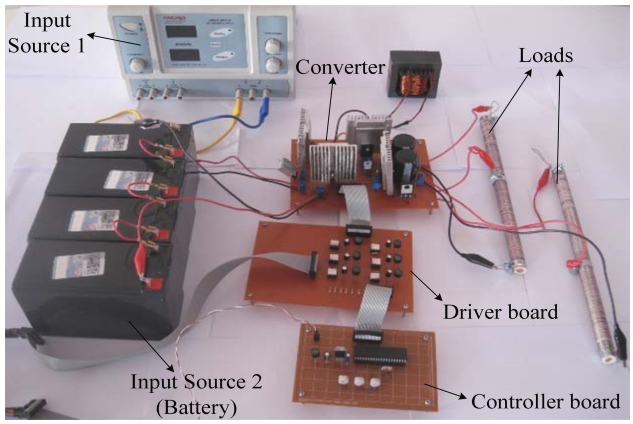

Fig. 18. Photograph of converter prototype.

are tracked the references values. In Fig. 16(b), battery current which is regulated to the desired value is shown. It is notable that the battery current in this mode has negative value which means the battery has been charged. Also, in this mode at a particular time ($t = 6.5$ s), the reference of the battery charging current is decreased suddenly from –0.9 A to –2 A. Also, at specific time ($t = 13$ s), output loads power are increased rapidly. In Fig. 17, the output voltages and battery current under these conditions are shown. As seen from this figure, the converter is controlled by designed compensators very well. It is worth noting that all converters have specific operating range. Also, power balance between inputs and outputs must be fulfilled.

VI. Experimental Results

In order to verify the effectiveness of the proposed converter, a low power range laboratory prototype was built as shown in Fig. 18. Two different input power sources utilized. A dc power supply and a 48-V battery consist of four series 12-V, 7.5 Ah lead–acid battery are employed in the prototype as the input sources. The parameters of the prototype are listed in Table I. For the experimental setup, the dc power supply is set at constant voltage values 35 V which can represent FC source. The control scheme is implemented by PIC18F452. The reference value of the output voltages are $V_{O1-\mathrm{ref}} = 80\,\mathrm{V}$ and $V_{O2-\mathrm{ref}} = 40\,\mathrm{V}$ and two resistive loads are used in the prototype. The experimental setup is examined in two different operation modes of converter. The experimental results for battery discharging and charging modes are described in detail as follows.

Battery discharging mode: In this mode, the reference current of the battery and output voltages are defined $I_{b-\mathrm{ref}} = 3\,\mathrm{A}$, $V_{O1-\mathrm{ref}} = 80\,\mathrm{V}$, *and* $V_{O2-\mathrm{ref}} = 40\,\mathrm{V}$, also $R_1 \cong R_2 \cong 35\ \Omega$(less than 35 Ω). Under this condition the output voltages of the converter is shown in Fig. 19(a). In this figure output voltage V_{O1} and total output voltage $V_T = V_{O1} + V_{O2}$ are shown. On the figure, by a circle the transition between battery discharging mode to battery charging mode is shown. The waveforms of voltages at the times before mode changing are related to battery discharging mode. It is obvious that the output voltages are regulated very well. The current drawn from battery is shown in Fig. 19(b). The average value of battery current is approximately equal to 3A. In Fig. 20(a) current which is drawn from source 1(dc power supply) is shown. Also, inductor current in this operation mode is shown in Fig. 20(b). By regulating of battery current, proper distribution of loads power between input sources is achievable. In this mode, $P_{\mathrm{in1}} \cong 150\,\mathrm{W}$, $P_b \cong 143\,\mathrm{W}$, $P_{O1} \cong 189\,\mathrm{W}$, and $P_{O2} \cong 47\,\mathrm{W}$.

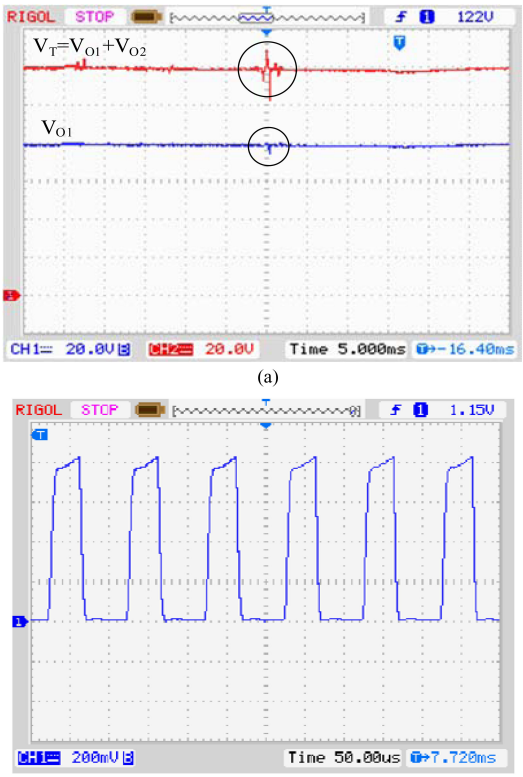

Fig. 19. Battery discharging mode. (a) Converter output voltages (20 V/div). (b) Drawn current from battery (2 A/div).

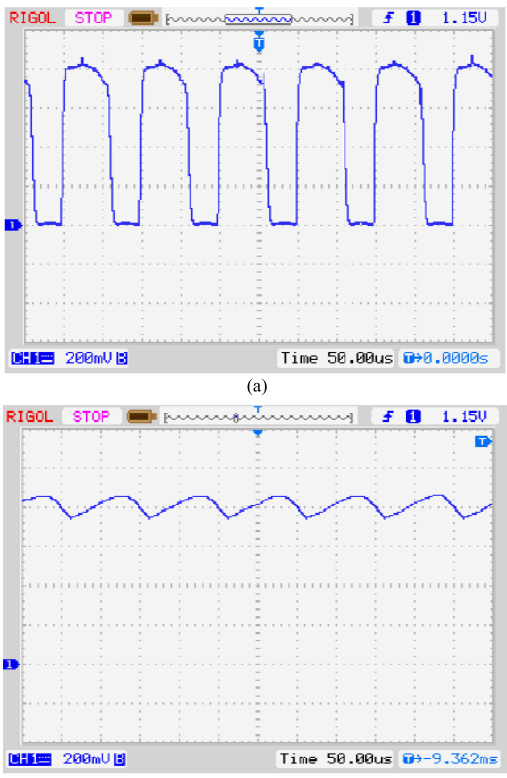

Fig. 20. Battery discharging mode (a) Drawn current from input source 1 (2 A/div). (b) Inductor current (2 A/div).

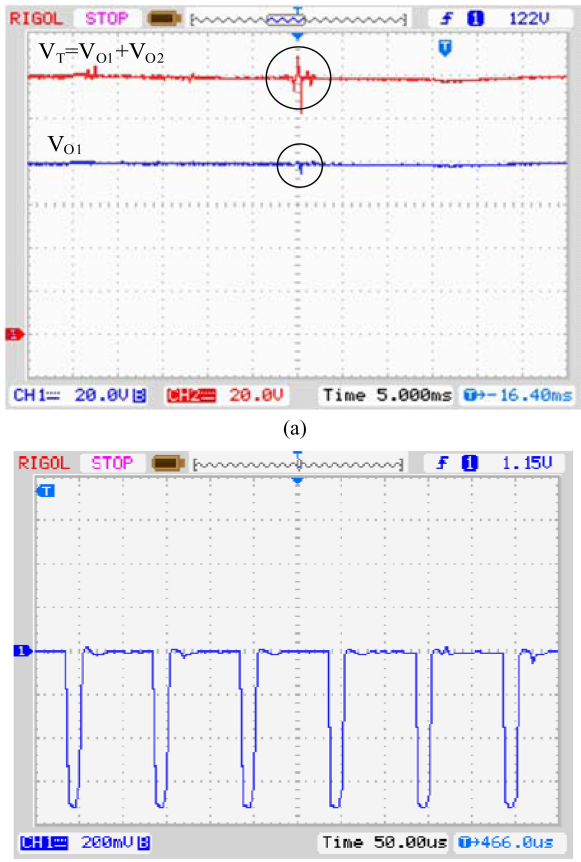

Fig. 21. Battery charging mode, (a) converter output voltages (20 V/div), (b) battery charging current (2 A/div).

Battery charging mode: In this mode, the loads power is low. So source 1 can supply loads and also charge the battery. In this mode, the reference of battery charging current and output voltages are defined $I_{b-\mathrm{ref}} = -0.9$ A, $V_{O1-\mathrm{ref}} = 80$ V *and* $V_{O2-\mathrm{ref}} = 40$ V, respectively, also $R_1 \cong R_2 \cong 70\ \Omega$ (less than 70 Ω). Under this condition, the output voltages of the converter are shown in Fig. 21(a). In this figure, the times after mode changing are related to battery charging mode. The battery charging current is shown in Fig. 21(b). In Fig. 22 inductor current is shown. It is worth noting that in this operation mode, current of source 1 is equal to inductor current. In this mode, $P_{\mathrm{in1}} \cong 214$ W, $P_b \cong 51$ W, $P_{O1} \cong 96$ W, and $P_{O2} \cong 25$ W. Also, the operation of the proposed converter from battery discharging mode to battery charging mode is investigated. First, the converter had been operated in battery discharging mode and then in appropriate time the load resistances have been increased. In battery discharging mode, the load resistances are $R_1 \cong R_2 \cong 35\ \Omega$ and in battery charging mode, the load resistances are $R_1 \cong R_2 \cong 70\ \Omega$. Also, the battery current reference which in battery discharging mode was 3 A is changed to –0.9 A. So, under such condition, the battery current and inductor current are shown in Fig. 23(a) and (b), respectively. Also, the output voltages transient in operation mode changing were shown in Figs. 19(a) and 21(a) by circles on the figures. At the

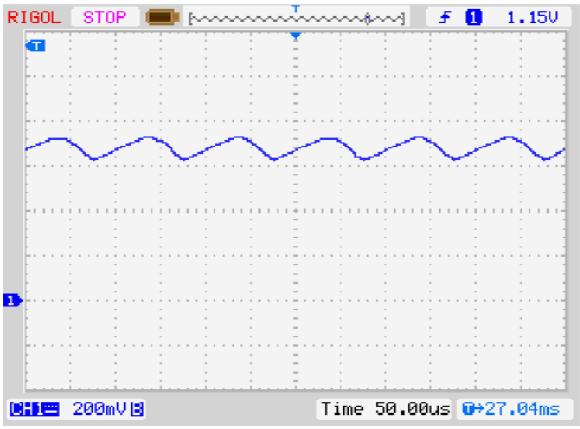

Fig. 22. Inductor current in battery charging mode (2 A/div).

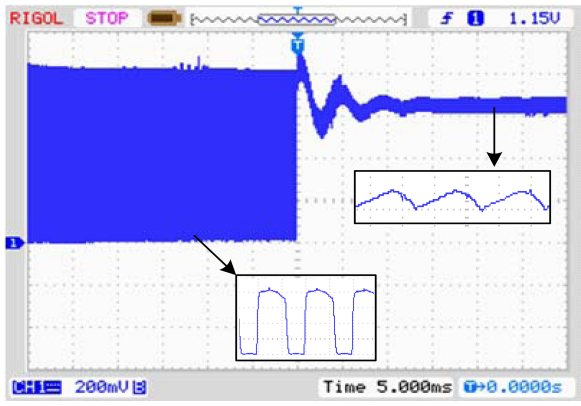

Fig. 24. Input source 1 (V_{in1}) current under operation mode changing from battery discharging to battery charging mode.

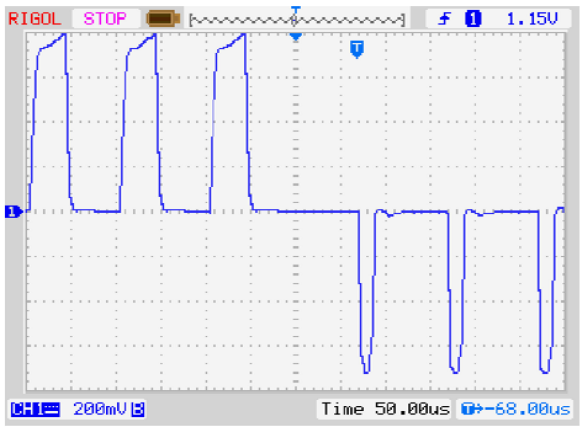

(a)

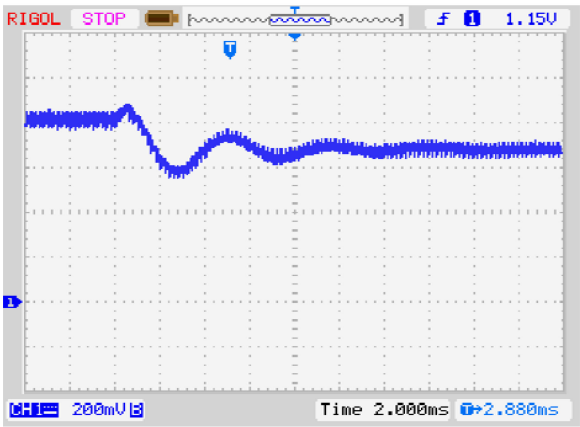

(b)

Fig. 23. (a) Battery current in battery discharging mode and battery charging mode (2 A/div), (b) inductor current transient in mode changing from battery discharging mode to battery charging mode (2 A/div).

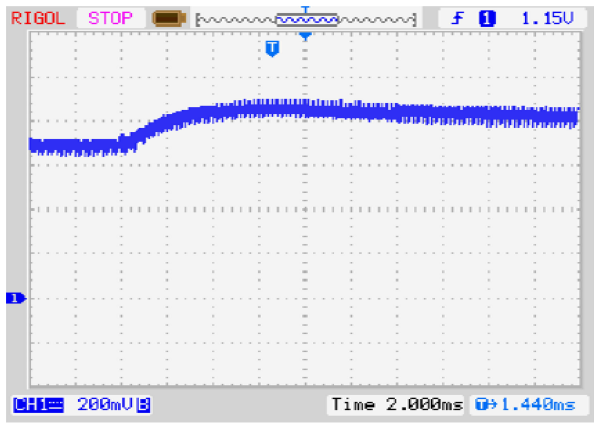

(a)

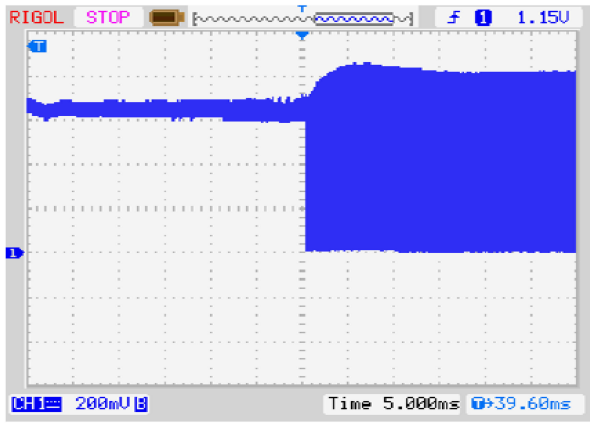

(b)

Fig. 25. (a) Inductor current in mode changing from battery charging to battery discharging mode (2 A/div), (b) input source 1 current in mode changing from battery charging to battery discharging mode (2 A/div).

times before transition time, the converter is in battery discharging mode and after transition time, the converter is in battery charging mode. It is obvious that against the operation mode changing and change of the loads the output voltages have been regulated to the desired values. In Fig. 24, the input source 1 current under mode changing from battery discharging to battery charging is shown. Also, for operation mode changing from battery charging mode to battery discharging mode similar results can be obtained. In Fig. 25(a) and (b), the inductor current and input source 1(V_{in1}) current in operation mode changing from

battery charging mode to battery discharging mode are shown, respectively.

VII. Conclusion

A new multiinput multioutput dc–dc boost converter with unified structure for hybridizing of power sources in electric vehicles is proposed in this paper. The proposed converter has just one inductor. The proposed converter can be used for transferring energy between different energy resources such as FC, PV, and ESSs like battery and SC. In this paper, FC and battery are considered as power source and ESS, respectively. Also, the converter can be utilized as single input multioutput converter. It is possible to have several outputs with different voltage levels. The converter has two main operation modes which in battery discharging mode both of input sources deliver power to output and in battery charging mode one of the input sources not only supplies loads but also delivers power to the other source (battery). For each modes, transfer functions matrices are obtained separately and compensators for closed loop control of the converter is designed. It is seen that under various conditions such as rapid rise of the loads power and suddenly change of the battery reference current, output voltages and battery current are regulated to desired values. Outputs with different dc voltage levels are appropriate for connection to multilevel inverters. In electric vehicles, using of multilevel inverters leads to torque ripple reduction of induction motors. Also, electric vehicles which use dc motors have at least two different dc voltage levels, one for ventilation system and cabin lightening and other for supplying electric motor. Moreover, in grid connection of renewable energy resources like PV, using of multilevel inverters is useful. Finally, operation of this converter was experimentally verified using low-power range prototype.

References

[1] X. Zhang and C. Mi, *Vehicle Power Management*, New York, NY, USA: Springer, 2011.

[2] M. Ehsani, Y. Gao, and A. Emadi, *Modern Electric, Hybrid Electric and Fuel Cell Vehicle Fundamentals, Theory and Design*, 2nd ed., New York, NY, USA: CRC Press, 2010.

[3] P. Thounthong, V. Chunkag, P. Sethakul, B. Davat, and M. Hinaje "Comparative study of fuel-cell vehicle hybridization with battery or supercapacitor storage device," *IEEE Trans. Veh. Technol.*, vol. 58, no. 8, pp. 3892–3905, Oct. 2009.

[4] L. Wang, E. G. Collins, and H. Li "Optimal design and real-time control for energy management in electric vehicles," *IEEE Trans. Veh. Technol.*, vol. 60, no. 4, pp. 1419–1429, May 2011.

[5] M. Zandi, A. Peyman, J. P. Martin, S. Pierfederici, B. Davat, and F. Meybody-tabar "Energy management of a fuel cell/supercapacitor/battery power source for electric vehicular applications," *IEEE Trans. Veh. Technol.*, vol. 60, no. 2, pp. 433–443, Feb. 2011.

[6] P. Thounthong, S. Pierfederici, and B. Davat, "Analysis of differential flatness-based control for fuel cell hybrid power source," *IEEE Trans. Energy Convers.*, vol. 25, no. 3, pp. 909–920, Sep. 2010.

[7] A. Peyman, S. Pierfederici, F. Meybody-tabar, and B. Davat, "An adapted control strategy to minimize dc-bus capacitors of parallel fuel cell/ultracapacitor hybrid system," *IEEE Trans. Power Electron*, vol. 26, no. 12, pp. 3843–3852, Dec. 2011.

[8] M. Michon, J. L. Duarte, M. A. M. Hendrix, and M. G. Simes, "A three port bidirectional converter for hybrid fuel cell systems," in *Proc. 35th Annu. IEEE Power Electron. Spec. Conf.*, Aachen, Germany, 2004, pp.4736–4741.

[9] J. L. Duarte, M. Hendrix, and M. G. Simoes, "Three-port bidirectional converter for hybrid fuel cell systems," *IEEE Trans. Power Electron.*, vol. 22, no. 2, pp. 480–487, Mar. 2007.

[10] H. Tao, A. Kotsopoulos, J. L. Duarte, and M. A. M. Hendrix, "Transformer-coupled multiport ZVS bidirectional DC–DC converter with wide input range," *IEEE Trans. Power Electron.*, vol. 23, no. 2, pp. 771–781, Mar. 2008.

[11] H. Tao, A. Kotsopulos, J. L. Duarte, and M. A. M. Hendrix, "Family of multiport bidirectional DC–DC converters," *Inst. Electr. Eng. Proc. Elect. Power Appl.*, vol. 153, no. 3, pp. 451–458, May 2006.

[12] H. Tao, J. Duarte, and M. Hendrix, "Three-port triple-half-bridge bidirectional converter with zero-voltage switching," *IEEE Trans. Power Electron.*, vol. 23, no. 2, pp. 782–792, Mar. 2008.

[13] H. Krishnaswami and N. Mohan, "Three-port series-resonant DC–DC converter to interface renewable energy sources with bidirectional load and energy storage ports," *IEEE Trans. Power Electron.*, vol. 24, no. 10, pp. 2289–2297, Oct. 2009.

[14] R. Ahmadi and M. Ferdowsi, "Double-input converter on h-bridge cells: derivation, small-signal modeling, and power sharing analysis" *IEEE Trans. Circuit Syst.*, vol. 59, no. 4, pp. 875–889, Apr. 2012.

[15] V. A. K. Prabhala, D. Somayajula and M. Ferdowsi, "Power sharing in a double-input buck converter using dead-time control," in *Proc. Energy Convers. Congr. Expo.*, 2009.

[16] Z. Li, O. Onar, and A. Khaligh, "Design and control of a multiple input DC/DC Converter for battery/ultra capacitor based electric vehicle power system" in *Proc. IEEE Twenty-Fourth Annu. Appl. Power Electron. Conf. Expo.*, 2009.

[17] K. Gummi and M. Ferdowsi, "Double-input DC-DC power electronic converters for electric-drive vehicles –topology exploration and synthesis using a single-pole triple-throw switch," *IEEE Trans. Ind. Electron.*, vol. 57, no. 2, pp. 617–621, Feb. 2010.

[18] S. M. Dehghan, M. Mohamadian, A. Yazdian, and F. Ashrafzadeh, "Dual-input dual-output Z-source inverter," *IEEE Trans. Power Electron.*, vol. 25, no. 2, pp. 360–368, Feb. 2010.

[19] T. Bhattacharya, V. S. Giri, K. Mathew, and L. Umanand, " Multiphase bidirectional flyback converter topology for hybrid electric vehicles," *IEEE Trans. Ind. Electron.*, vol. 56, no. 1, pp. 78–83, Jan. 2009.

[20] F. Nejabatkhah, S. Danyali, S. H. Hosseini, M. Sabahi, and S. A. Mozaffari Niapour, " Modeling and control of a new three-input DC–DC Boost converter for hybrid PV/FC/battery power system," *IEEE Trans. Power Electron.*, vol. 27, no. 5, pp. 2309–2325, May 2012.

[21] Y. C. Liu and Y. M. Chen, "A systematic approach to synthesizing multi-input DC–DC converters," *IEEE Trans. Power Electron.*, vol. 24, no. 1, pp. 116–127, Jan. 2009.

[22] O. C. Onar and A. Khaligh, "A novel integrated magnetic structure based DC/DC converter for hybrid battery/ultracapacitor energy storage systems," *IEEE Trans. Smart Grid*, vol. 3, no. 1, pp. 296–308, Mar. 2012.

[23] H. Wu, K. S. Ding, and Y. Xing, "Topology derivation of nonisolated three-port DC–DC converters from DIC and DOC," *IEEE Trans. Power Electron.*, vol. 28, no. 7, pp. 3297–3307, Jul. 2013.

[24] S. Danyali, S.H. Hosseini, and G. B. Gharehpetian, "New extendable single stage multi-input DC–DC/AC boost converter," *IEEE Trans. Power Electron.*, vol. 29, no. 2, pp. 775–788, Feb. 2014.

[25] A. Nami, F. Zare, A. Ghosh, and F. Blaabjerg, "Multi-output DC–DC converters based on diod-clamped converters configuration: Topology and control strategy," *IET Power Electron.*, vol. 3, pp. 197–208, 2010.

[26] A. A. Boora, A. Nami, F. Zare, A. Ghosh, and F. Blaabjerg, "Voltage-sharing converter to supply single-phase asymmetrical four-level diode-clamped inverter with high power factor load," *IEEE Trans. Power Electron.*, vol. 25, no. 10, pp. 2507–2521, Oct. 2010.

[27] J. D. Dasika, B. Bahrani, M. Saeedifard, A. Karimi, and A. Rufer, "Multivariable control of single-inductor dual-output buck converters," *IEEE Trans. Power Electron.*, vol. 29, no. 4, pp. 2061–2070, Apr. 2014.

[28] H. Behjati and A. Davoudi, "A MIMO topology with series outputs: An interface between diversified energy sources and diode-clamped multilevel inverter," in *Proc. Appl. Power Electron. Conf. Expo.*, 2012.

[29] H. Behjati and A. Davoudi, "A multi-port DC–DC converter with independent outputs for vehicular applications," in *Proc. Vehicle Power Propulsion Conf.*, 2011.

[30] R.W. Erickson and D. Maksimovic, *Fundamentals of Power Electronics*. 2nd ed., New York, NY, USA: Kluwer Academic Publisher, 2000.

Ali Nahavandi was born in Malayer, Iran, in 1983. He received the B.Sc. and M.Sc. degrees in electrical power engineering from the University of Tabriz, Tabriz, Iran, in 2006 and 2008, respectively. He is currently working toward the Ph.D. degree in electrical power engineering from the Faculty of Electrical and Computer Engineering, University of Tabriz, Tabriz, Iran.

His research interests include power electronic converters, renewable energy systems, and power quality. He currently focuses on the multiinput multioutput converters.

Mehrdad Tarafdar Hagh received the B.Sc. and M.Sc. degrees (with first honors) in power engineering in 1989 and 1992, respectively, and the Ph.D. degree in power engineering, in 2000, from the University of Tabriz, Tabriz, Iran.

He has been with the Faculty of Electrical and Computer Engineering, University of Tabriz from 2000, where he is currently a Professor. He has published more than 140 papers in power system and power electronics related topics. His research interests include power system operation, renewable energy, FACTS, and power quality.

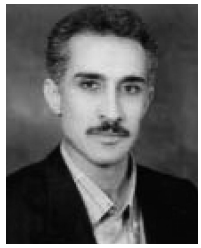

Mohammad Bagher Bannae Sharifian studied electrical power engineering at the University of Tabriz, Tabriz, Iran. He received the B.Sc. and M.Sc. degrees, in 1989 and 1992, respectively, and the Ph.D. degree in electrical engineering, in 2000, from the University of Tabriz.

In 1992, he joined the Department of Electrical Engineering, University of Tabriz, as a Lecturer. In 2000, he rejoined the Department of Electrical Power of the Faculty of Electrical and Computer Engineering of the University of Tabriz as an Assistant Professor. He is currently a Professor of the same department. His research interests include the areas of modeling and analysis of electrical machines, electric drives, liner electric motors, and electric and hybrid electric vehicle drives.

Saeed Danyali was born in Abdanan, Ilam, Iran in 1983. He received the B.Sc. degree in electronic engineering from the University of Yazd, Yazd, Iran, in 2005, and the M.Sc. and Ph.D. degrees in electrical power engineering from the University of Tabriz, Tabriz, Iran, in 2008 and 2013, respectively.

He has joined the University of Ilam, Iran, as an Assistant Professor in the Department of Engineering since Fall 2013. His research interests include the areas of renewable energy systems, power electronic converters, and electrical machines drives.